FIBRE DIFFRACTION REVIEW

Reports on Progress in Fibre Diffraction and Solution Scattering

A CCP13 / NCD Publication

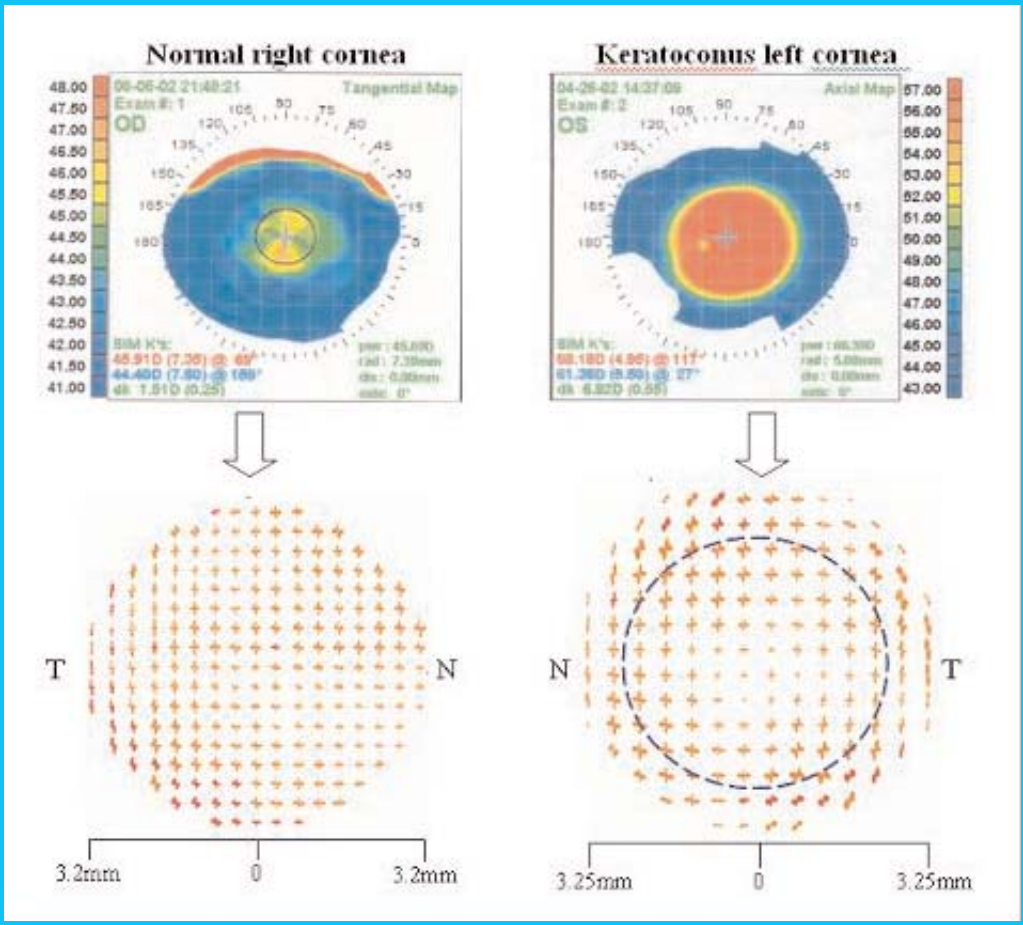

Application of fibre X-ray diffraction to analysis of abnormal corneas

Volume 14 **April 2006**

FDR April 2006 CONTENTS Volume 14

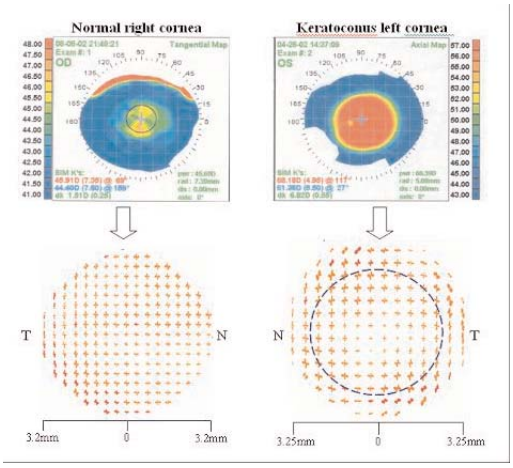

Cover Image: Application of fibre X-ray diffraction to analysis of abnormal corneas. Videokeratography images (top) and corresponding scanned array vector plot maps (below) from X-ray fibre patterns of a normal cornea (left) and a keratoconus cornea (right). For details see Hayes et al. (this volume).

Editorial Office:
Editor: Prof John Squire, Biological Structure and Function Section,
Imperial College London, SW7 2AZ.
Production: Ms Toun Baruwa, Biological Structure and Function Section,
Imperial College London, SW7 2AZ.

From the Chairman

Dear Friends,

In all, this has been a difficult year for CCP13. This is almost entirely due to the lack of success I had in obtaining funding from BBSRC (and EPSRC) for a three year funding of future activities. What was most galling was that I believe that we had made great leaps forward with a project proposal that was supported by facilities such as DIAMOND, ISIS and the ESRF who were willing to put significant funding into the project. Cardiff and Reading Universities also committed themselves to financial support; in total over £200,000 was pledged. I am led to believe that the grant was rejected on the grounds that CCP13 activity is not critical to the community it serves. I obviously disagree. The establishment of DIAMOND and the additional capabilities that will be available in the near future at TS2 mean that software support for data reduction and modelling is needed more than ever. However, the days of major core grant funding for CCP projects are probably over for the foreseeable future.

We therefore have to consider a way forward in the near future that requires evolution of CCP13 and proves to future funders that we are re-engaged with a vibrant community using software produced under the CCP13 banner to do world class science. Plans to move toward this position are already taking shape. Individual groups including my own are seeking (and receiving!) grant funding to work on specific projects for software development. Working as a collective, and defining specific projects based around specific scientific goals, may be part of the answer; it appears to work for some other CCP groups. It also looks as if some of the funding pledged in the original grant application may be used to employ researchers in software development, which is excellent news. In addition, I intend in the immediate future to apply for "Tools and Resources" funding in order to establish a dialogue with all users, and potential users, of the community. If this is successful, expect me to visit you in 2006/7!

I'd like to end on a positive note, and I hope that the 80+ of you who attended the Cardiff meeting from all corners of the globe will all agree that it was a great success and that you now think the weather here in Wales is fantastic. I certainly enjoyed hosting the event and look forward to a repeat performance in 2007 to celebrate the inauguration of (and to show off) my new School Building. Finally, I'd like to thank all the members of the executive who made crucial contributions to the grant proposal, it seemed like such a good idea at the time.

Tim Wess
Cardiff University, March 2006

From the Editor

Dear All,

You will have seen from the Chairman's report that CCP13 is suffering from a lack of central funding at the moment. This also has had its impact on the production of Fibre Diffraction Review. However, in my view, having something in our field like Fibre Diffraction Review to inform non-crystalline diffractionists of both software and hardware developments and to provide a forum for young scientists to present their work in abstracts from the CCP13 Workshops and as selected, expanded poster prize papers is a good way of fostering a healthy and thriving community. For this reason it is my intention to keep editing and producing Fibre Diffraction Review for the foreseeable future. The Journal will at least appear annually in electronic format on the CCP13 website (www.ccp13.ac.uk) and if possible will also be produced and circulated in hard copy. However, production of hard copy is expensive and production this way will depend on the demand from CCP13 members and the amount of funding available.

The present volume includes updates on our own CCP13 software suite, namely FibreFix, which I encourage you to use for yourselves since it is becoming more and more powerful for many different NCD applications, and also, courtesy of Nick Terrill, on progress with the NCD part of Diamond.

John Squire
Imperial College London, March 2006.

Fibre Diffraction Review 14, 3 - 4, 2006 doi: 10.1382/fdr.2006.1401

Meeting Report - CCP13 2005 Workshop, Cardiff

As Chairman of CCP13 it was a delight to be able to hold the annual workshop in Cardiff, it also gave the executive the opportunity to mark the occasion by mapping out the future directions for CCP13. The weather held out for most of the time and lulled all 80 of us into a false sense of security before the rain on the final day. With an audience from four continents, we had an excellent spread of scientific diversity. I had asked in advance for speakers to focus on the commonality that should exist for all of us in the process of getting from scattering signal to structure. Most of us made this a focal point of our presentations and this was well received. Presentations ranged from Rudi Winter(Aberysytwth) on the use of Anomalous signals in small angle X-ray scattering to Tom Irving ((Illinois/ APS) highlighting his most recent work on synchronous behaviour in insect flight muscle and Clair Baldock (Manchester) using SAXS to unravel the shapes of segments within elastic proteins.

We maintained our fundamental interest in fibre diffraction with presentations by, among others, Gerald Stubbs (Vanderbildt) on plant virus particles, and Naoto Yagi (spring8) on Microbeam diffraction from hair and skin.

Poster Prizes were judged by Oskar Paris and Naoto Yagi, the joint winners were Felicity Eakins (Imperial) and Sally Dennis (Cardiff) for their posters entitled "Time Resolved X-ray Diffraction Studies of Active Bony Fish Muscle: Analysis using the New CCP13 Program FibreFix" and "The Relationship between Surface Corneal Topography and Stromal Collagen Organisation in Normal and Keratoconus Corneas", well done to them and their collaborators.

The conference dinner was well received and everyone got to sample some traditional Welsh fayre. Most of us now also know what goes on at a Welsh funeral wake, well at least until they are asked to leave!

Tim Wess & Carlo Knupp, Cardiff

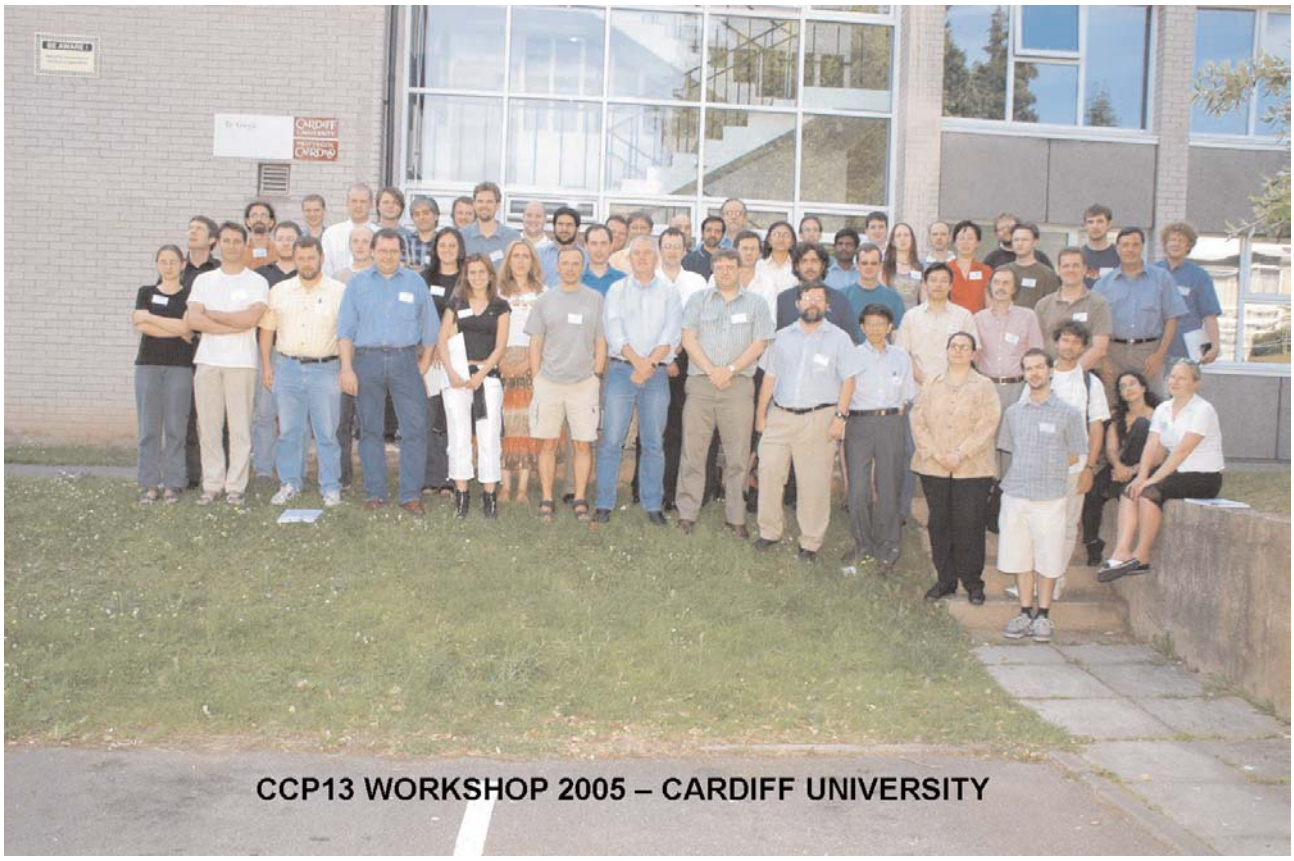


CCP13 WORKSHOP 2005 – CARDIFF UNIVERSITY

Fibre Diffraction Review 14, 5 - 9, 2006 doi: 10.1382/fdr.2006.1402

Small Angle X-ray Scattering on Diamond

Nick Terrill

Diamond Light Source Ltd, Rutherford Appleton Laboratory, Chilton, Didcot,
Oxfordshire OX11 0DE, UK

Abstract

Building of the new UK Diamond synchrotron at the Rutherford Laboratory is now well advanced and beamlines are being assembled. Here progress on the non-crystalline diffraction facilities I22 (being implemented) and HATSAX (possible) is outlined, together with plans for on-line data analysis.

Update on Beamline I22

[1] Optics Design

Design work for the optics hutch is nearing completion with only some diagnostic components still outstanding. Initial beam diagnostics will be performed by a pair of FMB designed X-ray photon beam position monitors (Figure 1). These will be installed into I22's front end and will give the beamline an accurate indication of incident beam position and stability.

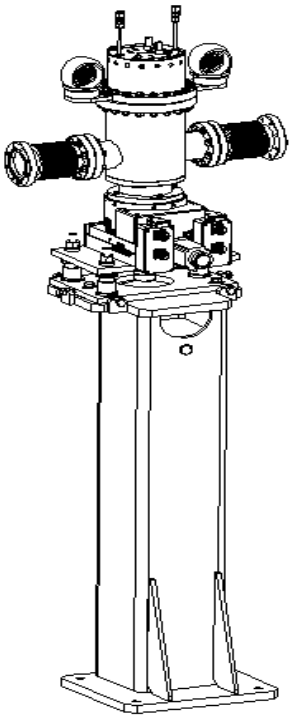

Figure 1 *- FMB XBPM, two will be installed into I22's front end giving information on beam position and angle.*

In the optics and experimental hutches the diagnostics will comprise both beam observation and measurement through in-house designed diagnostic systems (Figure 2). In time these will be incorporated into the feedback systems for I22 to ensure that the user community get optimum performance from the beamline.

Figure 2 *- Monochromatic beam Diagnostic assembly. This will give information about position, intensity and shape of the beam incident through the optics on I22.*

[2] End Station

The end station design is progressing well with contracts let for the Sample platform (IDT - Figure 3a) and detectors (HOTSAXS, HOTWAXS and RAPID with CCLRC). The Small Angle X-ray Scattering Detector mounting platform will allow both detectors to be available to the user community during a scheduled experiment with minimal changeover time (Figure 3b). The HOTWAXS detector will be mounted on an A-frame above orbit plan, the nosecone for the detector has been designed such that alternative front pieces can be mounted to minimise air gaps for different sample environments.

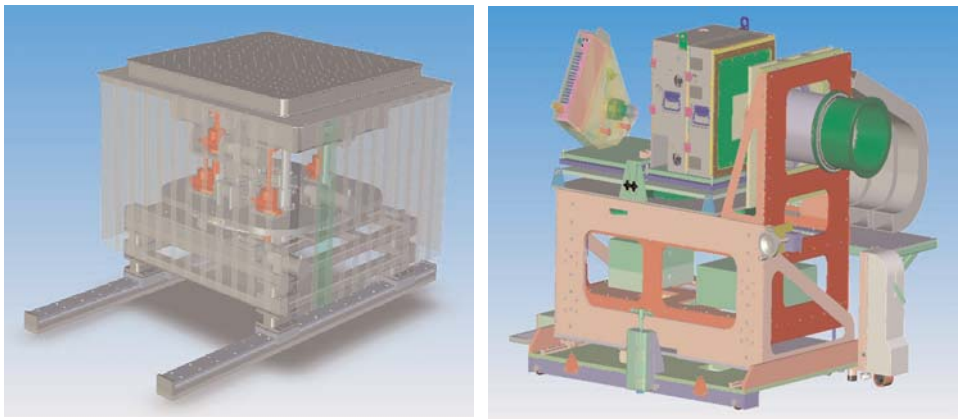

Figure 3 *- Left) Sample platform with breadboard for easy mounting of sample environments. This assembly is also adaptable to include spacers to vary the height of the platform grossly. Right) Small Angle X-ray Scattering Detector platform. Also included on this assembly is the beamstop. Independent movement of detector and beamstop is possible.*

The beamline compliment of sample environments will be discussed over the coming months but is likely to include DSC, capillary heater, stop flow cells and liquid cells. Sample changers can be accommodated on the standard sample platform and users are encouraged to contact the beamline team to discuss their requirements at the earliest possible convenience. The sample platform has x-y translation (±100mm) and limited pitch (±5°) and yaw (±10°) for sample alignment purposes.

[3] Building I22

IDT designed the primary silts for I22 (Figure 4). These are at Diamond Light Source and are ready to be installed once the cabins and services contract is complete.

The monochromator from Oxford Danfysik is due for delivery in April. The characteristics of the fixed exit monochromator will allow I22 to deliver anomalous scattering experiments in the range 4-20keV without the need for translation of the sample stage.

The K-B mirror system from Accel has been delivered and will be installed in the optics hutch towards the middle of May this year. The properties of the vertical focusing mirror (VFM) have been tested at Elettra (Figure 5) and indicate that I22 will have excellent performance from its focusing system (slope error <1.3?m without bimorph correction).

The monochromatic slits have also been delivered to Diamond Light Source (Figure 6). We have worked with ADC to produce a design that should, not only act as an excellent slit system (blade roughness <1?m), but also provide feedback. The blades have been electrically isolated and therefore it should be possible to measure beam position via a drain current measurement. This information can again be fed back to the optics system to ensure stable sampling.

[4] Installation of I22

Anyone who has been to Diamond over the last 12 months will have seen that tremendous progress has been made on all fronts. I recommend that anyone interested takes a look at http://www.diamond.ac.uk/default.htm regularly. I22 is also taking shape. On the experimental floor the x-ray hutches have been installed and we are nearing the completion of the cabins and services installation (Figure 7).

Figure 4 *- Left) Primary Slits Assembly. Right) one of the water cooled blades prior to assembly.*

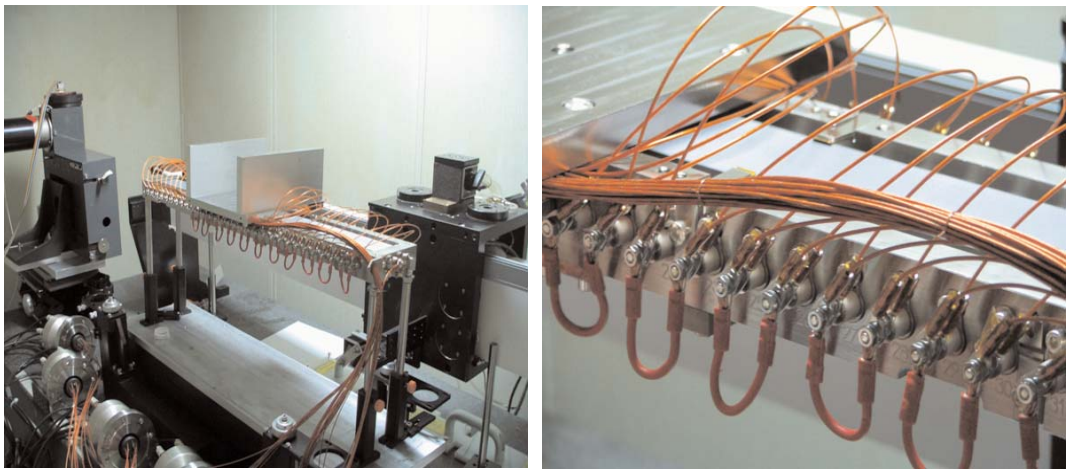

Figure 5 *- Two views of the VFM for I22 during testing at Elettra. The pictures give a view of the 32 electrode connections. For these tests they were shorted together.*

Figure 6 *- Monochromatic slits 2, you can see the electrical feed through's alternately spaced with the motor mechanism around the flange into which the slits are mounted..*

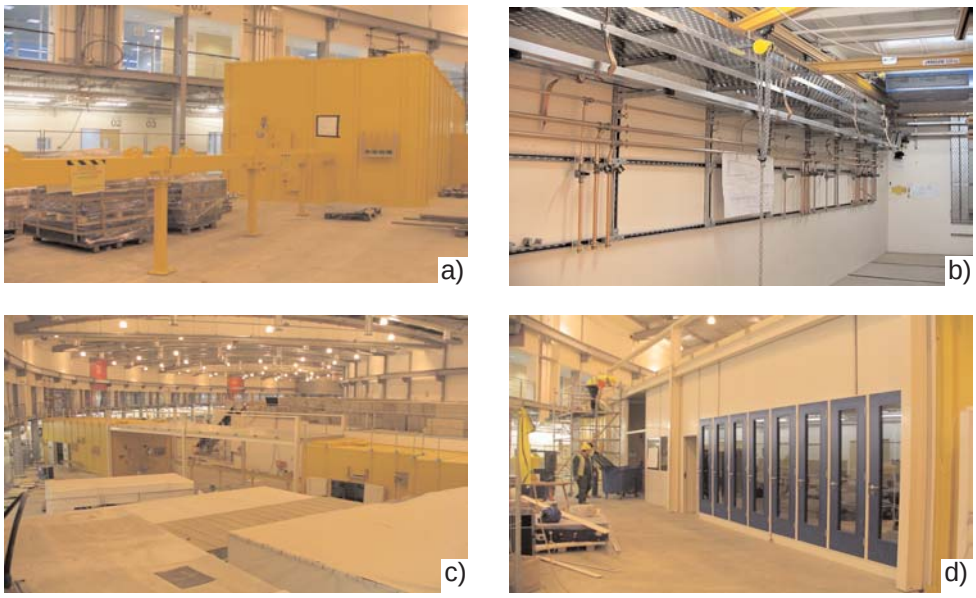

Figure 7 *- Views of I22 during installation a)Transfer line showing Experimental hutch, b) internal detail of Optics hutch showing tray work and services supply pipes, c) Overview of I22 area, optics hutch to right and experimental hutch to left. Installation of the steel-work to support the user and control cabins is underway in the middle d) View showing the Controls and Instrumentation Area (CIA) areas and in back-ground the User cabin..*

The CIA will house the control racks for motors, vacuum and data handling. Regular photographic updates of construction progress can be found at: http://www.diamond.ac.uk/Beamlines/Beamlineplan/I22/Progress.htm.

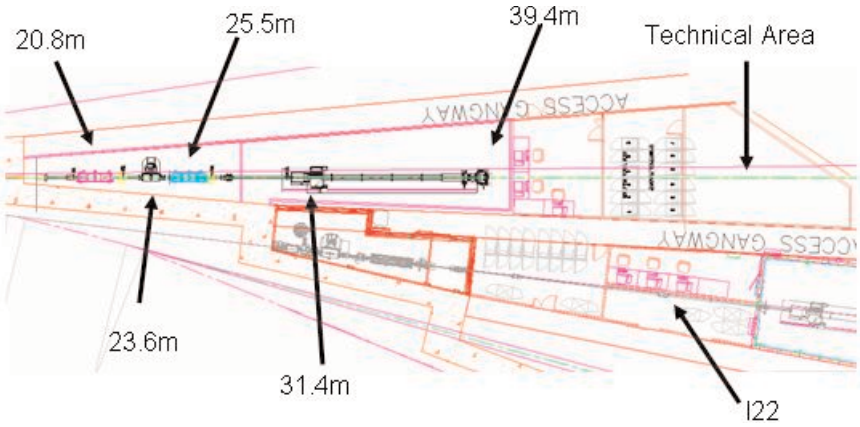

Figure 9 *Possible layout for HATSAXS alongside I22.*

[5] Commissioning of I22

Commissioning with X-rays will commence later this year after the installation of our U25 in-vacuum undulator in August. Commissioning without beam is expected to be an ongoing process as soon as the first equipment is installed in June 2006.

[6] Data reduction - Data Analysis

It will be possible to carry out data reduction on line for both 1D and 2D data on I22. Building on the GDA software that is being rolled out across all Diamond beamlines we have developed simple data reduction screens that will take the users through the basic steps, data normalisation, detector response correction and experimental background subtraction. Working with live data from the current experiment and using only a few parameters that can be adjusted it will give a very quick view of the data so that decisions can be made during beamtime rather than offline later. These simple mode screens are complimented by a scripting engine that will permit more complicated operations to be performed. Figure 8 shows two screenshots for the package. Figure 8a illustrates how simple mode for 1D data will look. The illustration has 100 curves of simulated scattering intensity from spheres of different diameters. Figure 8b illustrates how the 2D display will look. The illustration here displays the same 1D data as in Figure 8a displayed as a 2D plot but could be of any 2D data set. It is planned to "pipe" the data from these programs into any user community data analysis packages including all of those from CCP13.

Progress on developing a HATSAXS on Diamond

There is a proposal to build a second beamline for Small Angle X-ray Scattering (HATSAXS) on Diamond using a bending magnet source. If all goes well the beamline will be operational by 2011. The layout in Figure 9 shows how a possible HATSAXS solution may look on the Diamond experimental floor. It will be located alongside I22 to allow the two beamlines to share resources.

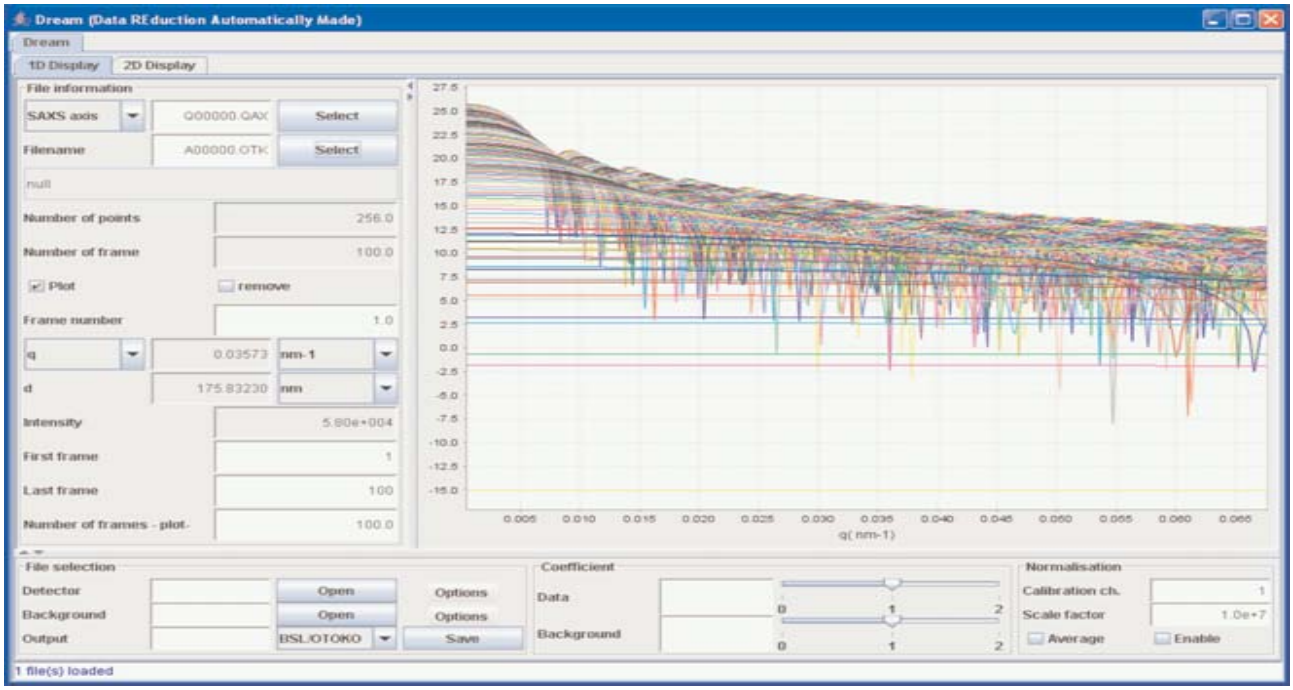

Figure 8a*: shows the envisaged 1D panel.*

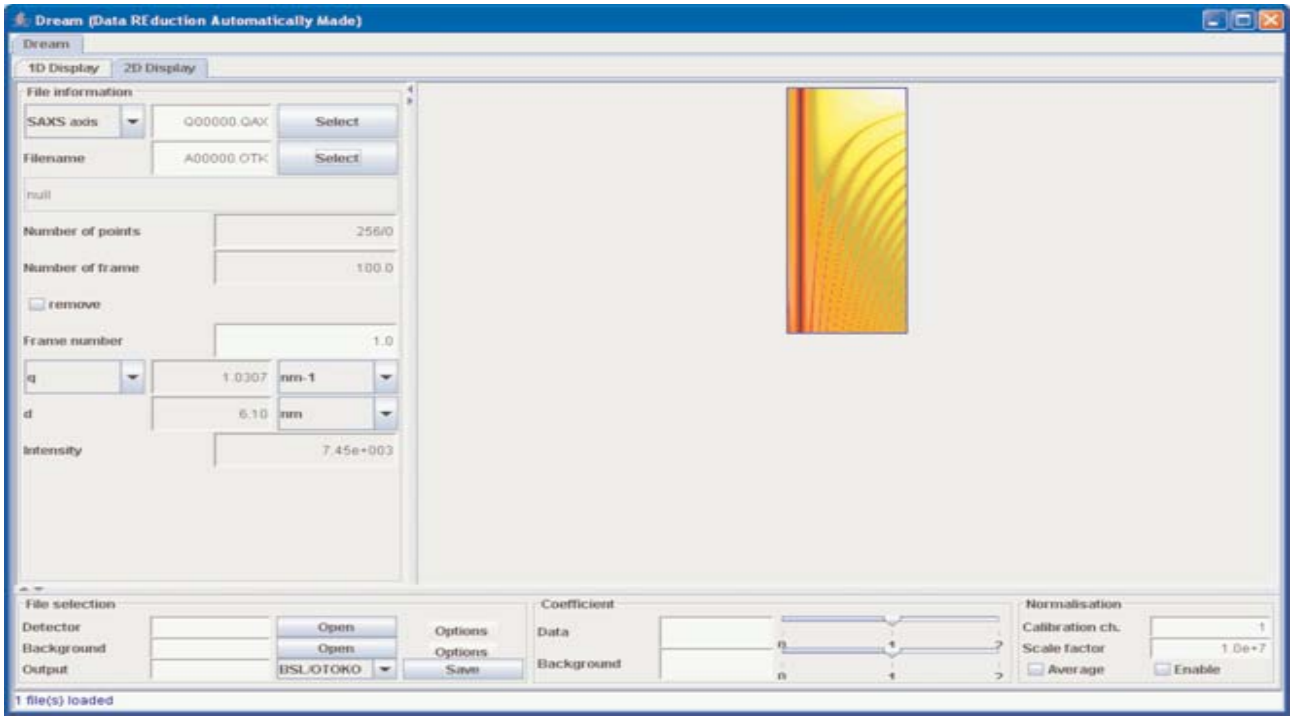

***Figure 8b**: shows the envisaged 2D panel*

	SRS line6	**Diamond dipole 2:1**	**Diamond dipole 3:1**
Source	10 pole MPW 2.0T	Dipole 1.4T	Dipole 1.4T
Mirror length	1.2m	1.2m	1.2m
Mirror width	0.14m	0.14m	0.14m
Horizontal fan	1mrads	0.6mrads	0.6mrads
Vertical fan	0.35mrads	0.35mrads	0.35mrads
X-ray energy	10keV	10keV	10keV
Beam current	200mA	300mA	300mA
Mirror slope error	0.5 arc-sec FWHM	0.5 arc-sec FWHM	0.5 arc-sec FWHM
Sagittal crystal thickness variation	15% over 60mm	15% over 60mm	15% over 60mm
Focal spot size sigma (HxV) at 10keV	0.42mm x 0.09mm	0.07mm x 0.06mm	0.05mm x 0.07mm
Focal spot divergence sigma (HxV) at 10keV	0.60mrad x 0.23mrad	0.39mrad x 0.16mrad	0.59mrad x 0.27mrad
Flux in focus	3.6 x 10^{12} photons/sec	2.1 x 10^{12} photons/sec.	2.1 x 10^{12} photons/sec

***Table 1** - Performance Comparison for SRS line 6 with Diamond Dipole at 2:1 and 3:1 demagnification*

Table 1 shows the possible performance of a beamline built this way. The flux is down on the comparable beamline, 6.2, at the SRS, but beamsize and divergence are also smaller.

Fibre Diffraction Review 14, 10 - 14, 2006 doi: 10.1382/fdr.2006.1403

The CCP13 FibreFix Program Suite and Recent Updates

Ganeshalingam Rajkumar[1], Hind A. AL-Khayat[1], Felicity Eakins[1], Carlo Knupp[1,2] and John M. Squire[1]

1. Biological Structure & Function Section, Imperial College London, Exhibition Road, London SW7 2AZ, UK
2. Structural Biophysics Group, School of Optometry and Vision Sciences, Redwood Building, Cardiff University, Cardiff, CF10 3NB, UK.

Abstract

Many users are currently applying the new CCP13 software package FibreFix to their own research. This is both testing the software under varied real world conditions and also, in some cases, leading to requests for the software to be modified or enhanced for the specific needs of the user. So, both through user requests, the correction of bugs, and the already planned enhancement of FibreFix, a number of changes have been made to the original FibreFix suite both to improve it and to make it more powerful. These changes are implemented in the current version (FibreFix 1.3). They include addition of new 'BSL' operations and improvement in the input and control of some of the original BSL functions. We outline these developments here.

Following the initiation of CCP13 in the early 1990s, a number of independent programs were developed, particularly by Dr. Richard Denny, to process and analyse data in non-crystalline diffraction patterns (Denny, 1993; Denny and Shotton, 1999; Denny et al., 1998). These programs, the most important of which in their latest incarnations are termed XCONV, XFIX, FTOREC and LSQINT, were designed to build on the existing BSL program developed by Joan Bordas and Geoff Mant at the Daresbury Laboratory. They were built around what became the standard BSL file format. All of these programs were written for UNIX platforms and, although being very effective, they were rather non-intuitive and cumbersome in their use. The CCP13 Committee therefore decided to link these programs in an integrated, user-friendly, suite firstly in a PC Windows environment. In addition, the original programs required parameters determined in one process to be carried forward manually into the next routine, a rather laborious process. The new program suite was therefore required to integrate the original programs into a single 'suite' where parameters that have already been determined in one part of the analysis are automatically carried forward to the next without user intervention (Squire et al., 2003). The resulting suite, originally known as ICE but now called FibreFix, is implemented for the Microsoft Windows platform (He et al., 2004; Rajkumar et al., 2005). It includes the functionality of the programs XCONV, XFIX, FTOREC and LSQINT and also all of the routines which were originally part of the UNIX BSL program. It is intended that the whole FibreFix suite will eventually be ported to Java, or an equivalent platform, so that it can also be used on any UNIX or LINUX machine.

Here we describe a number of new features that have been implemented in the current FibreFix program (FibreFix Version 1.3) and we discuss planned future developments.

Loading of files

The program XCONV was originally the way of converting images from detector format into the BSL format used by the CCP13 software. Loading an image was often an interactive process. FibreFix has now been developed so that the XCONV functionality is automatically present. Image files in known formats can either be loaded using the normal 'open' function under the 'file' drop down menu, or can simply be 'dragged and dropped' into the image window. The FibreFix program automatically recognises many standard detector formats and image formats and will open the files automatically without user interaction unless there are some uncertainties in, for example, the image array size. As discussed later (Figure 6), several image files can easily be loaded at the same time and can be treated as successive 'frames' of a single image.

Improvements and updating of 'old' BSL functions in FibreFix 1.3

Many of the old BSL functions have been implemented in FibreFix and in several cases improved. Initially FibreFix created plots using the BSL functions HOR (integrate HORizontally), VER (integrate VERtically), SEC (SECtor integration), RIN (Radial INtegration) and TIP (Time series Intensity Plot) by selecting appropriate regions of the diffraction pattern using the mouse, then right clicking on the mouse to display the plot in a new

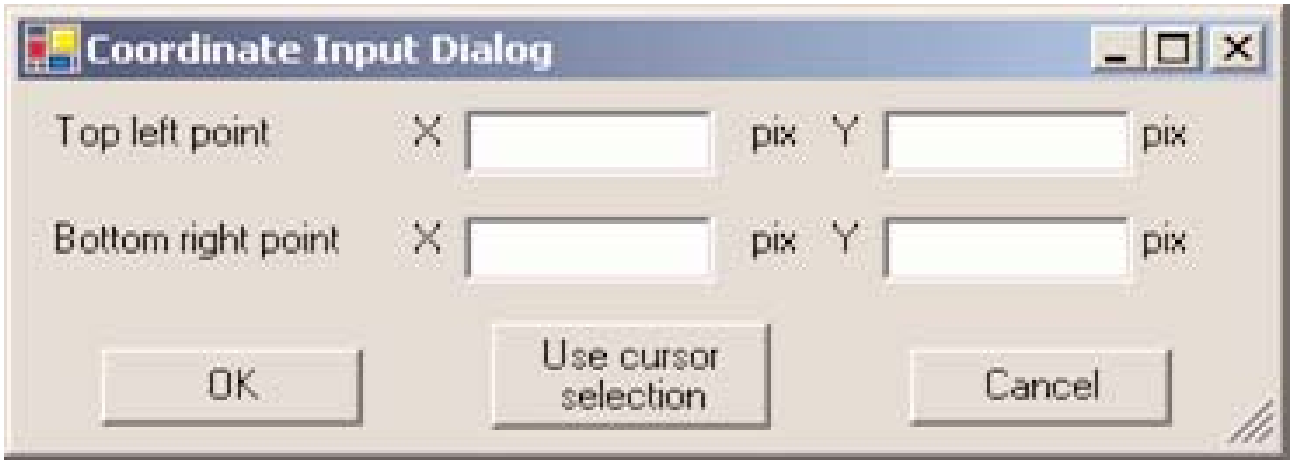

Figure 1: *The new query box which appears when it is necessary to select precise parameter ranges for intensity integrations in FibreFix.*

popup window. However, it was difficult to be precise in positioning the mouse to select an exact area of the image, especially if it is necessary to analyse the same regions in many different patterns using the same limits of integration. These plot regions can now be selected in an alternative way by entering the exact pixel coordinates of the area for integration in a popup window as shown below (Figure 1). Clicking on OK will plot the graph in a separate popup window as before.

Another development is such that the program plotting functions have been updated to plot one-dimensional logs when the image is displayed in a log scale. Also a number of bugs in these routines have been fixed.

New BSL functions in FibreFix

FibreFix 1.3 has been updated with several new added BSL functions such as ADF (ADdition of a series of Frames), CAL (CALibration file normalisation) and CIN (Circular INtegration) which are used as below. There has also been a modification to the use of the ROTation function ROT:

[1] ADF: The ADF function adds sets of image Frames together in a time series. By specifying the Frames to be added in the input window, specific groups of Frames in a time series can be added together. Note that only where several Frames are being added is it necessary to include those Frame numbers in the ADF query box. In the example below (Figure 2) new Frame 1 is the same as old Frame 1, new Frame 2 is the sum of old Frames 2 to 4, new Frames 3 and 4 are replaced by old Frames 5 and 6, new Frame 5 is replaced by the sum of Frames 7 to 12 and so on.

As a separate application of the ADF function, several independent exposures (files) of exactly the same repeated experiment can be added together by inputting them as a set of files using the input procedure in Figure 6. They

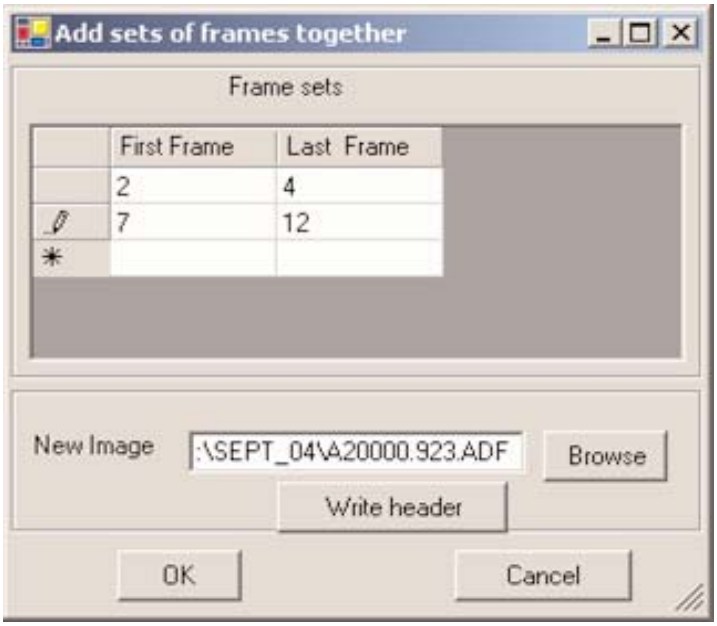

Figure 2: *The query box which appears when using the BSL 'ADF' function in FibreFix.*

are then stored in the program as if they are successive Frames in a multiframe file and can be added together using the ADF function.

[2] CAL: The CAL function plots a modified calibration file by dividing the calibration value for each frame by the user input exposure time of each frame in a time series. This allows the measurement which has been saved in the calibration file to be normalized with respect to exposure time so that a sensible plot can be made of the calibration data against frame number. In order to explain the application of CAL, we give an example below from one of our own time-resolved X-ray diffraction experiments on fish muscle (Figure 3). In the recorded exposures the frame duration changed as in Table 1:

[3] CIN: The CIN function plots circular integration profiles in a selected radial range of a diffraction pattern. By

Frames up to	Exp time (ms)
2	100
152	1
153	100
254	4

Table 1: *Frame numbers and exposure times in a time-resolved X-ray diffraction experiment on contracting bony fish muscle. Frames 1 and 2 each had exposure times of 100 ms, Frames 3 to 152 had exposure times of 1 ms, Frame 153 had an exposure of 100 ms, and Frames 154 to 254 had exposures times of 4 ms. These translate into the entry in the CAL function input query box in BSL as in Figure 3.*

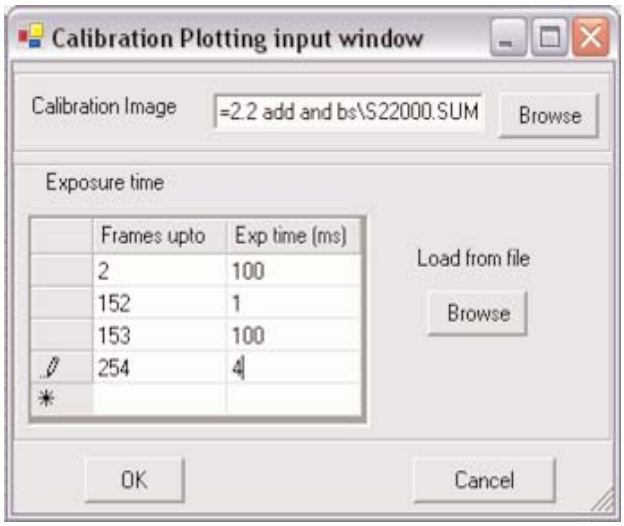

Figure 3: *The query box which appears when using the BSL 'CAL' function in FibreFix.*

Figure 4: *Application of the new BSL 'CIN' (circular integration) function in FibreFix. This selects and plots the observed intensity around an annulus in the observed diffraction pattern and can reveal details of the degree of orientation in a polymer sample.*

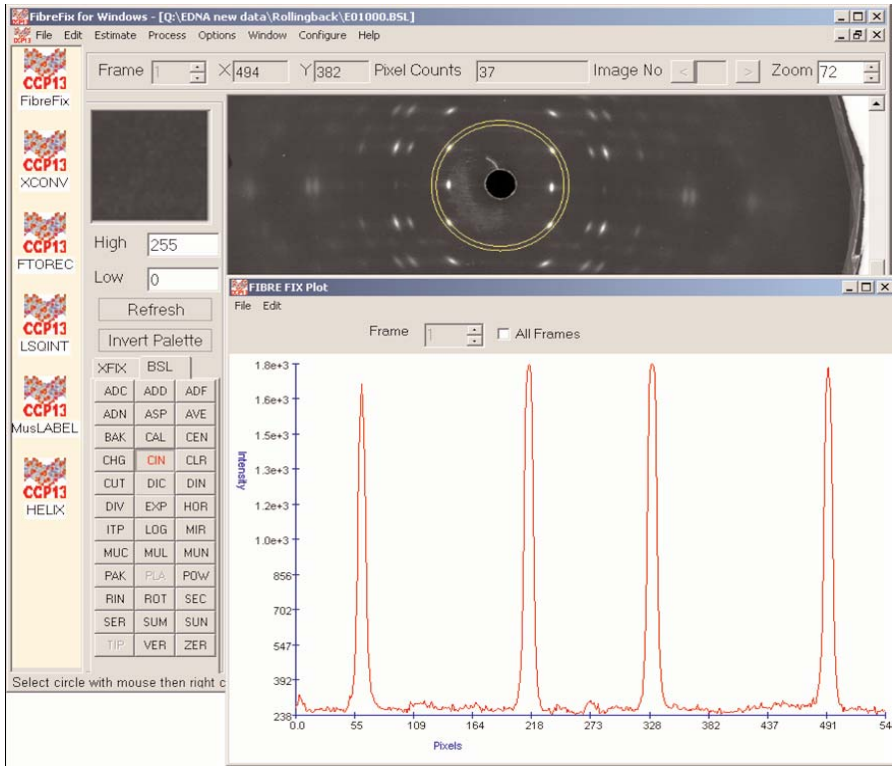

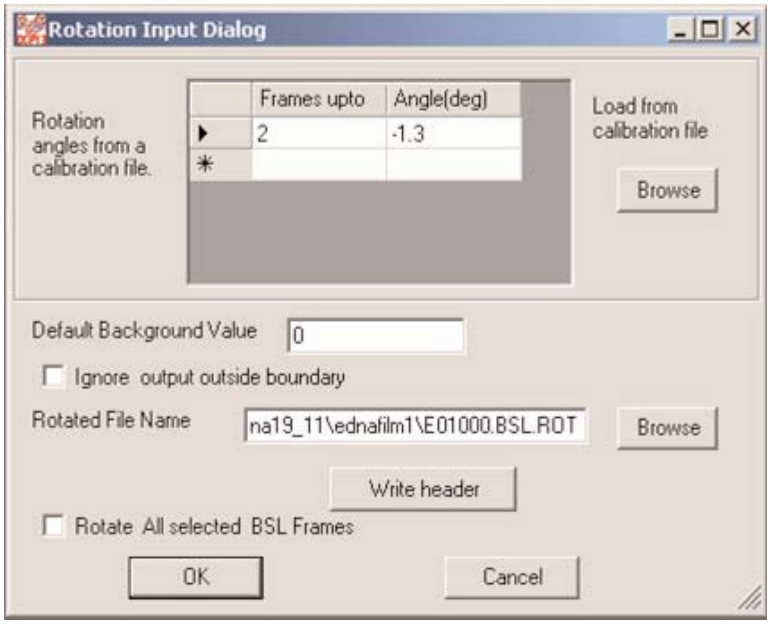

Figure 5: *The new query box that appears when the BSL function 'ROT' is opened. It allows for variable correction of the pattern rotations throughout a time-series.*

selecting the CIN function on the BSL tool tab one can plot the required intensity profile around a circle either by mouse clicking or by inputting the centre, radius and radial width of the annular area to be integrated. Then by right-clicking on the mouse the annular intensity profile is plotted (Figure 4). This can be used, for example, for estimating the degree of orientation (texture) in partially ordered synthetic polymer samples.

[4] ROT: The ROT tool has been updated to allow for slight variations in absolute orientation of the fibre axis of a single sample during a time series. It applies different angles of rotation to different time frames (Figure 5).

Multiple files can be selected and processed together
Multiple files can be selected in FibreFix and operations can then be carried out on all the files selected as the multiframe BSL file. Multiple files can be selected by holding the CTRL key while clicking the necessary files (Figure 6). Alternatively files can be selected by clicking the first file to select and then, while holding down the SHIFT key, clicking the last file to select. The program assumes all the selected files are of same file format and the same dimensions.

Estimation of Spacings and Unit Cell Parameters
A new feature of FibreFix 1.3 is the ability to determine approximate peak spacings in the pattern once the wavelength and camera length have been put into the Parameter file. Using the Get Spacings option under XFIX, the user can click on a peak of interest of unknown spacing, right click and automatically generate spacing estimates. These are printed in the text box at the bottom of the FibreFix window. The estimated 'real' spacings given are the Bragg spacing d and, for 'vertically' oriented fibre specimens, the radial (row line) and axial (layer line) spacings of the peak. From these spacings the approximate dimensions of the unit cell can be defined.

Modelling Programs
As well as stripping fibre diffraction data and analysing other kinds of non-crystalline diffraction patterns, it is important to have tools with which to model possible candidate structures. Two simulation programs have been written, the program HELIX (Knupp and Squire, 2004) to model simple helical structures and also the program MusLABEL (Squire and Knupp, 2004) to model the specific kinds of structures that are found in striated muscles. The least-squares molecular refinement program LALS is also in the process of being updated for CCP13 (Arnott et al., 1969).

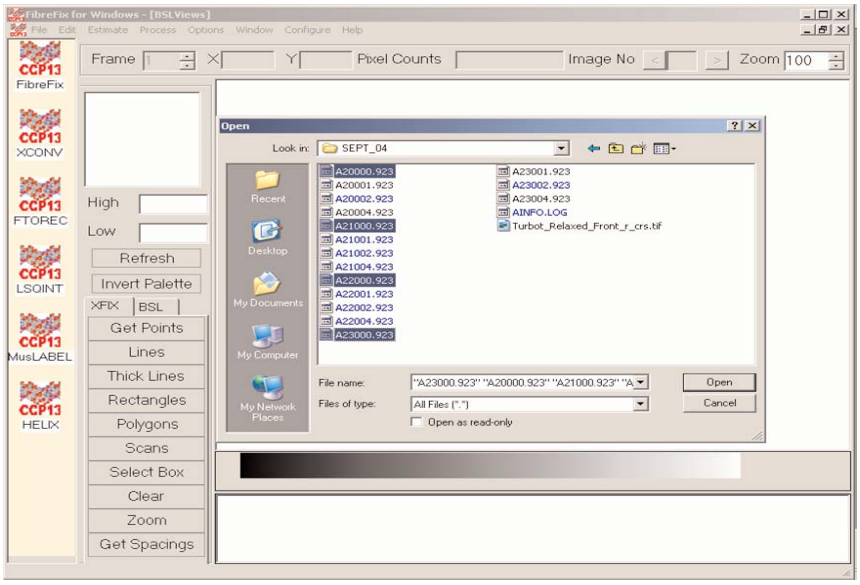

Figure 6: *Selection of multiple files for common processing within BSL.*

The future: Proposed additional updates

In the near future a number of additional features will be added to FibreFix. These include additional routines within the BSL processing package such as:

CNV **C**o**NV**olute two files.

CON Generate a **CON**tour map.

FFT Perform 2-D Fast Fourier Transform on an image.

GAU Generate a 2-D **GAU**ssian function.

IFT Calculate the **I**nverse **F**ourier **T**ransform.

SUR **SUR**face plot (isometric projection).

It is also hoped that new background subtraction procedures will be included in **FTOREC** and **LSQINT**. The full program will also include a 2D or 3D Fourier synthesis package based on data output from **LSQINT**.

Finally we hope that before too long updated versions of the 1D analysis programs **XFIT** and **XOTOKO** will also be incorporated within **FibreFix**. When we have a final package which we believe fulfils a great deal of the needs of the non-crystalline diffraction community we will implement the whole **FibreFix** suite in Java. Please also note that there are several **FibreFix** tutorials on the CCP13 website (www.ccp13.ac.uk) which refer to particular kinds of user applications.

Acknowledgements

We are indebted to the BBSRC and EPSRC for several grants supporting the CCP13 activity (recently #28/B10368 & #28/B15281) and specifically the development of FibreFix for CCP13 and also the Wellcome Trust (# 061729) for support of CK while various FibreFix tools were being implemented. We also acknowledge contributions from Andrew He during the early part of FibreFix development (the suite was then called ICE) and the many users who have made suggestions about new features to incorporate into FibreFix or who have pointed out bugs.

REFERENCES

Arnott, S., Dover, S.D. & Wonacott, A.J. (1969) "Least-squares refinement of the crystal and molecular structures of DNA and RNA from X-ray data and standard bond lengths and angles". Acta Cryst. B25, 2192-2206.

Denny, R.C (1993) Integration of fibre diffraction patterns: FDTOREC and LSQINT. Fibre Diffraction Review 2, 5-8.

Denny, R.C. & Shotton, M.W. (1999) CCP13 Software Development Fibre Diffraction Review 8, 14-19.

Denny, R.C., Shotton, M.W. & Forsyth, V.T. (1998) CCP13 Software Development. Fibre Diffraction Review 7, 40-44.

He, A., Rajkumar, G., Forsyth, T. & Squire, J.M. (2004) Report on CCP13 software developments: Production of an integrated CCP13 environment (ICE) for Windows. Fibre Diffraction Review 12, 21-23.

Knupp, C. & Squire, J.M. (2004) HELIX: A helical diffraction simulation program. J. Appl. Cryst. 37, 832-835.

Rajkumar, G., AL-Khayat, H.A., Eakins, F., He, A., Knupp, C. & Squire, J.M. (2005)
FibreFix - A New Integrated CCP13 Software Package. Fibre Diffraction Review 13, 11-18.

Squire, J.M. & Knupp, C. (2004) MusLABEL: A Program to Model Striated Muscle A-band Lattices, to Explore Crossbridge Interaction Geometries and to Simulate Muscle Diffraction Patterns. J. Mus. Res. Cell Motil. 25, 423-438.

Squire, J.M., AL-Khayat, H.A., Arnott, A., Crawshaw, J., Denny, R., Diakun, G., Dover, S.D., Forsyth, V.T., He, A., Knupp, C., Mant, G., Rajkumar, G., Rodman, M.J., Shotton, M. & Windle, A.H. (2003) New CCP13 software and the strategy behind further developments: Stripping and modelling of fibre diffraction data. Fibre Diffraction Review 11, 7-19.

Fibre Diffraction Review 14, 15 - 21, 2006 doi: 10.1382/fdr.2006.1404

The Relationship between Surface Corneal Topography and Stromal Collagen Organisation in Normal and Keratoconus Corneas

S Hayes[1], C Boote[1], Y Huang[2] and K M Meek[1]

1. Structural Biophysics Research Group, School of Optometry and Vision Sciences, Cardiff University, Redwood Building, King Edward VII Avenue, Cardiff CF10 3NB, UK

2. Department of Ophthalmology, Great Wall Hospital of PLA, 28 Fuxing Road, Beijing P.R. China

Abstract

A specific arrangement of collagen provides the cornea with its strength, shape and transparency. As a result, abnormalities in the structural organisation of stromal collagen have been implicated in several corneal diseases, such as keratoconus. The aim of this study is to examine the relationship between corneal structure and specific keratoconus shape changes to improve our understanding of the mechanism by which the disease progresses. High-angle X-ray fibre diffraction was used to map the preferred orientation and distribution of fibrillar collagen in a normal cornea and two excised keratoconus corneal buttons. The X-ray diffraction data were examined alongside videokeratographic images of the same corneas taken prior to surgery. Abnormalities in collagen orientation and mass distribution were seen in both of the keratoconus corneal buttons. A relationship appeared to exist between the size and shape of the cone and the extent of structural alterations in the stroma of keratoconus corneal buttons. The results are consistent with a theoretical mechanism of keratoconus progression which involves enzyme action and inter-fibrillar and inter-lamellar slippage, causing a loss of some tissue mass and a redistribution of the remaining tissue mass within the corneal button region.

Keywords: *Cornea, keratoconus, X-ray scattering*

Introduction

The cornea, which is a tough, transparent tissue covering the front of the eye, acts as the main refractive component of the ocular system; its precise curvature determines the quality of the image formed on the retina. The stroma forms 90% of the cornea and is composed primarily of water and Type I collagen.

Within the stroma, parallel collagen fibrils are arranged in layers (lamellae) which travel in all directions within the plane of the cornea but predominantly in the superior-inferior and nasal-temporal directions.

The specific arrangement of collagen provides the cornea with its shape, transparency and strength [1, 2]. As a result of this, abnormalities in collagen organisation have been implicated in several corneal diseases, one of which is keratoconus, a condition that is characterised by a progressive thinning and steepening of the cornea, resulting in severe, irregular astigmatism (Figure 1B). Keratoconus affects between 4 and 200 people per 100, 000 [3], and is the second most common cause of corneal transplant surgery in the UK [4].

The advent of computer-assisted corneal topography analysis (videokeratography) in recent years has greatly facilitated the early diagnosis and monitoring of keratoconus, by providing the clinician with information about the precise shape of the cornea in the form of a colour coded contour map of corneal dioptric power.

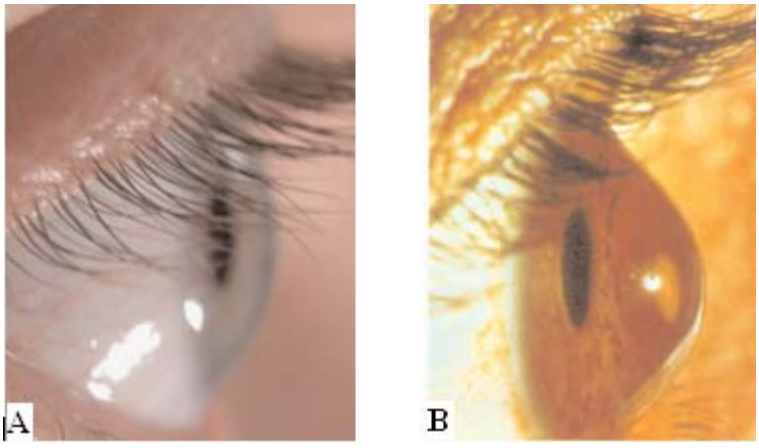

Figure 1. *The side profile of a normal cornea (A) and a keratoconus cornea (B).*

Once diagnosed, the majority of cases may be successfully treated through the use of glasses and hard contact lenses. However, in 10-20% of keratoconus patients, severe corneal scarring at the apex of the cone results in a permanent decrease in visual acuity that can only be restored by means of a corneal transplant.

The present study examines the interesting relationship between corneal structure and shape by examining X-ray diffraction derived information about the arrangement and distribution of collagen in normal and keratoconus corneas alongside videokeratographic images of the same corneas.

Methods

Tissue samples

Two unscarred keratoconus corneal buttons of 6.5 mm diameter were obtained at the time of penetrating keratoplasty from Great Wall Hospital (Beijing, Japan) with the patients' consent. Keratoconus button 1, which was from the left eye of a 17-year-old male, had a maximum corneal dioptric power of 72.79D. Keratoconus button 2, which was from the left eye of a 26-year-old male, had a maximum corneal dioptric power of 81.10D. Both buttons were tagged at the 12 o'clock position with a nylon suture before being preserved in 2.5% formalin. A normal human eyeball (removed within 3 hours post mortem) was also tagged at the 12 o'clock position and stored in 2.5% formalin. Immediately prior to data collection the cornea with a 2mm scleral rim was carefully dissected from the normal human globe using a scalpel.

Videokeratography

Prior to surgery, videokeratographic images of corneal surface dioptric power were recorded using an EyeSys topography system (EyeSys Vision, Texas, USA). A grid overlay of 1 x 1 mm squares was superimposed onto the topography map to highlight the position, size and shape of the cone. In the case of the normal post mortem eyeball, videokeratography was performed within 2 hours after ennucleation. The same colour and dioptric interval scale was used for each map, whereby warm colours represent the regions of highest dioptric power (the steepest regions) and cold colours indicate the areas of lowest dioptric power (flatter regions).

X-ray diffraction data collection

All X-ray diffraction data were collected on Station 14.1 at Daresbury Synchrotron Radiation Source (Warrington, UK), using a 0.2 x 0.2 mm beam with a wavelength of 0.1488 nm. The samples were wrapped tightly in clingfilm (to prevent tissue dehydration during data collection) before being placed (in their correct orientation) into an airtight sample holder enclosed between two sheets of Mylar (Dupont-Teijin, UK). The sample holder was then carefully secured onto a computer-operated translation stage with the most anterior side of the cornea facing the X-ray beam. High-angle X-ray diffraction images were collected over the entire sample at regular intervals of 0.4 mm in the case of the normal cornea with scleral rim and 0.5 mm for each of the keratoconus buttons. The X-ray exposure time of 75 seconds per image used for the normal cornea was increased to 180 seconds for the thinner keratoconus corneal buttons in order to maximise the signal to noise ratio. X-ray diffraction images (Figure 2A) were recorded on a Quantum 4R CCD detector (ADSC, Poway, CA) placed 150 mm behind the sample.

X-ray diffraction data analysis

The angular distribution of scatter intensity around the intermolecular reflection (Figure 2A) was measured to form a 0-360 distribution pattern (Figure 2B) using Optimus 6.5 (Media Cybernetics, UK) image analysis software and Excel (Microsoft, UK). To take into account variations in beam intensity and exposure time between samples, the intensity profile for each image was normalised against the average X-ray intensity (recorded by an ion chamber at the time of exposure) multiplied by the exposure time. The intensity profile was then folded to improve the signal to noise ratio; this was possible without the loss of any data, due to the centro-symmetric nature of X-ray fibre diffraction patterns. At this stage, the total area under the intensity profile (i.e. the total scatter) is proportional to the total mass of fibrillar collagen in the path of the X-ray beam (Figure 2B). This can be divided into two components; isotropic scatter arising from a background of collagen fibrils equally disposed in all directions within the plane of the cornea and aligned scatter from fibrils that adopt a preferred orientation [5]. Removal of the isotropic scatter leaves only the scatter from preferentially aligned lamellae, which we will refer to as 'aligned collagen' (Figure 2C).

The area under each intensity profile (Figures 2B and 2C) was summed to produce a numeric value of scatter intensity for both total collagen mass and aligned collagen mass. The scatter intensity from aligned collagen as a proportion of the total collagen scatter was calculated to form a ratio (index of orientation), whereby an index of 1 indicates that all of the collagen at that particular point in the tissue is preferentially aligned and an index of 0 means that the collagen is distributed equally in all directions within the plane of the cornea. Two-dimensional contour maps showing the distribution of total collagen scatter and the index of orientation were formed by plotting each calculated intensity value/index onto a grid relating to corneal position. On the assumption that the keratoconus buttons and the normal cornea were similarly hydrated, the scatter distribution contour plots represent the relative distribution of collagen mass within each sample. By presenting aligned collagen mass as an index of orientation, the reduced stromal thickness of the keratoconus corneas is taken into account, thereby highlighting any differences in aligned collagen mass distribution between the normal and keratoconus corneas.

To show the preferred orientation of aligned collagen molecules at a specific point in the tissue, the intensity profile of aligned collagen scatter was shifted by 90º (to account for the fact that the high-angle equatorial reflection appears at right angles to the fibril axis) and then converted to a vector plot (Figure 2D) [5]. The distance from the centre of a vector plot to the edge, at any given angle, represents the intensity of aligned collagen scatter from collagen molecules oriented in that particular direction. As the collagen molecules are aligned roughly parallel to each other and the fibril axis, the orientation of the molecules can be said to reasonably represent the direction of the collagen fibrils at that position within the corneal stroma. The individual vector plots were compiled onto a grid relating to corneal position to form a 'vector plot map', showing the preferred orientation of aligned collagen across each sample.

Results

Figure 3 shows the index of orientation in the central 10 mm of a normal right cornea. The index of orientation increases in all four quadrants of the peripheral cornea, but most prominently in the superior-nasal and inferior-temporal quadrants. Within the central 6.4 mm region (highlighted by a dashed blue line in Figure 3), the increase in the index of orientation is seen only in the superior-nasal and inferior-temporal quadrants. As a non-superimposable mirror symmetry of collagen mass distribution has been shown to exist between the normal left and right cornea [7], it is possible for the purposes of this study to compare the distribution of collagen mass in two left 6.5 mm keratoconus buttons to the distribution of collagen mass in the central 6.4mm region of a normal right cornea (Figure 4).

Videokeratography

Figure 4 (A-C) shows the corneal surface dioptric power of the normal cornea and two keratoconus corneas. In contrast to the normal cornea, which has a maximum dioptric power of 45.69D (Figure 4A), both keratoconus corneas have regions of very high dioptric power (66.39D in keratoconus button 1 and 69.33D in keratoconus button 2) which highlight the position, size and the shape of the cone (Figure 4B and C). Keratoconus button 1 has a large centrally positioned round cone which measures 5.08mm

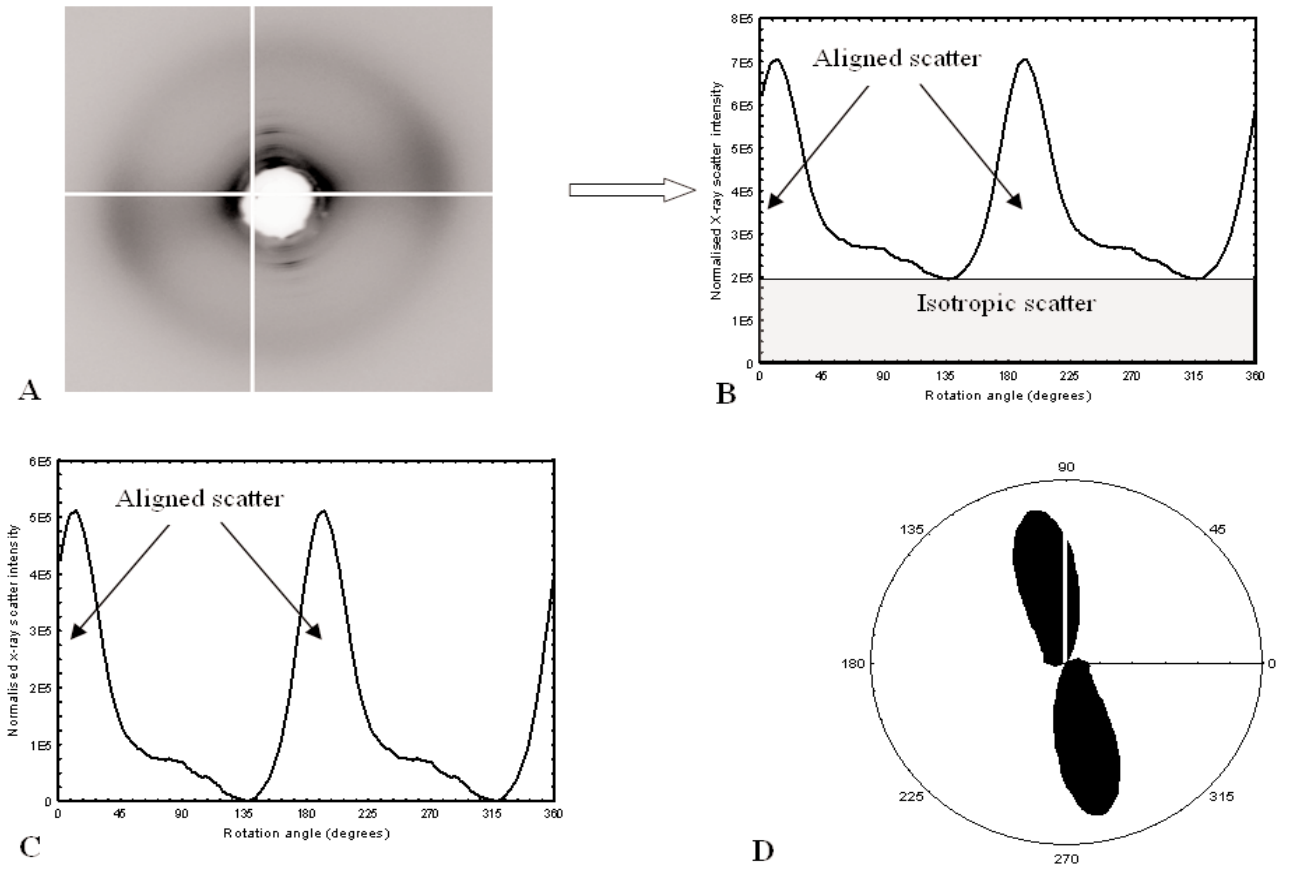

Figure 2. *A high angle X-ray scattering pattern from corneal collagen (A). The profile of total collagen scattering intensity (from both isotropic and preferentially aligned collagen) (B) and preferentially aligned collagen scatter only (C), are shown as a function of angular position around the X-ray scatter pattern. The profile of aligned collagen scatter intensity is converted to a vector plot (D), taking into account the fact that X-rays are scattered at right-angles to the fibril axis. The distance from the centre of a vector plot in any given direction is representative of the amount of collagen fibrils preferentially orientated in that particular direction.*

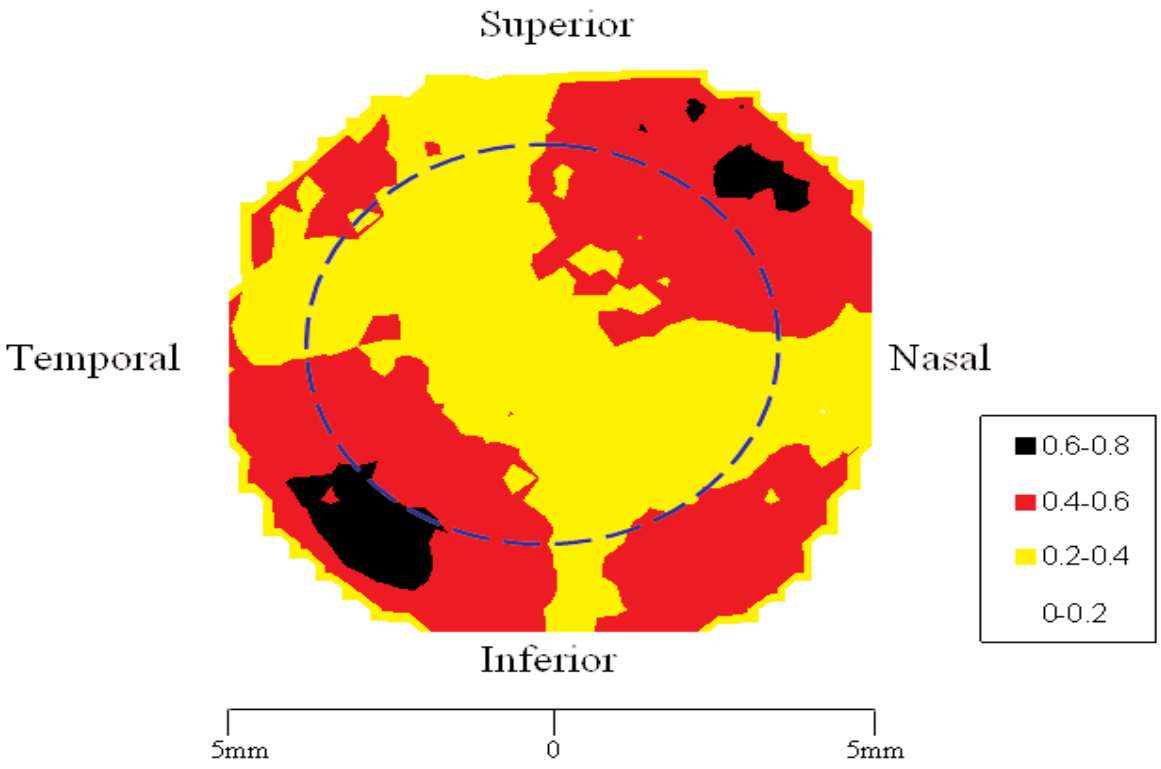

Figure 3. *A contour map showing the index of orientation (aligned/total collagen mass) in the central 10mm of a normal right human cornea. The index of orientation increases in all four quadrants of the peripheral cornea, but predominantly in the superior-nasal and inferior-temporal quadrants. The central 6.4 mm region is highlighted by a blue dashed line; this region will be used for comparison with keratoconus buttons 1 and 2.*

in radius (when shown as a 2D projection) and keratoconus button 2 has a smaller inferior-temporally located oval cone of 4.87mm radius.

Preferred collagen orientation

In Figure 4 (D-F) vector plot maps show the preferred orientation of aligned collagen in the central 6.4 mm region of the normal cornea and in the central 6.5 mm region of keratoconus buttons 1 and 2. In the normal cornea more aligned collagen fibrils lie in the superior-inferior and nasal-temporal directions than in any other which gives rise to the characteristic cross shaped vector plots seen in previous studies of normal human corneas [6, 8]. Towards the edge of the 6.4 mm region, the preferred orthogonal orientation is gradually 'swamped' by additional aligned collagen lying tangentially to the edge of the cornea (Figure 4D).

The normal preferred orientation of collagen in the central cornea is lost to varying extents in both of the keratoconus corneal buttons (Figure 4E and F). In keratoconus button 1, which exhibits a large round cone (Figure 4B) the normal orthogonal orientation is lost throughout most of the 6.5 mm button (Figure 4E). In the case of kerato conus 2, which has an oval-shaped cone (Figure 4C), the preferred orientation of aligned collagen is only altered at the apex of the cone (Figure 4F). In both cases, the disruption to normal preferred collagen orientation is greatest at the apex of the cone and decreases with distance from the apex.

Total collagen mass distribution

Contour plots showing the distribution of total collagen mass in the normal right cornea and the two left keratoconus buttons are shown in Figure 4 (G-I). When shown on the same intensity scale as the keratoconus corneal buttons, the distribution of collagen mass in the normal cornea appears to be fairly uniform across the central 6.4 mm region. In both keratoconus buttons the total collagen mass is lower than normal within the region of the cone. This is as one might expect since maximal stromal thinning is known to occur within the cone region of keratoconus corneas.

Index of orientation

The index of orientation in the central 6.4 mm of the normal right cornea is highest in the superior-nasal and inferior-temporal quadrants where between 40 and 60% of the total collagen is preferentially aligned (Figure 4J). As mentioned previously, the increase in the index of orientation occurs predominantly in the superior-nasal and inferior-temporal quadrants of both left and right corneas [7]. However, within the central 6.5 mm of keratoconus button 1 (which has a round, centrally located cone; Figure 4B) the index of orientation increases to a similar extent in all four quadrants (Figure 4K).

In the central 6.5mm region of keratoconus button 2 (which has an oval, inferior-temporally located cone) (Figure 4C), the index of orientation increases only in the superior-nasal and inferior-temporal quadrants; this is as one might expect for a normal left cornea based on the findings of Boote and colleagues [7]. However, in the case of keratoconus button 2, the index of orientation is higher than normal and occurs well within the main optical zone of the cornea (Figure 4L).

Discussion

There are at present two main theories regarding the mechanism of stromal thinning in the cone region of keratoconus corneas; one is a loss of collagen mass through tissue degradation [9], and the other is a redistribution of collagen mass by means of inter-fibrillar or inter-lamellar slippage [10]. Despite much research, the exact mechanism by which the cornea thins and steepens in keratoconus is still unknown. However, for the first time, we are able to link specific keratoconus shape changes to structural alterations within the stroma by examining X-ray diffraction data alongside videokeratographic images of surface corneal power.

As collagen has greatest tensile strength along its fibril axis and is preferentially orientated in most tissues in the direction of greatest stress [11], this has prompted suggestions that the preferred orthogonal orientation of fibrils in the superior-inferior and nasal-temporal directions of the normal cornea (Figure 4D) may resist the stress exerted by the extra-ocular muscles and so prevent tissue distortion during eye movement [6, 8, 12].

In both keratoconus corneas, the normal orthogonal preferred orientation of collagen was lost within the cone region and in the case of keratoconus button 1 (which had the largest cone); a disturbed arrangement of collagen was also observed throughout the remainder of the 6.5 mm button. Consistent with previous studies [3, 12-15], the most striking changes in collagen orientation were observed at the apex of the cone and gradually decreased with distance from the apex. As the amount of collagen alignment in the superior-inferior and nasal-temporal directions of the normal cornea is highest in the posterior stroma [16], these findings provide evidence that major structural alterations occur in the posterior stroma of advanced keratoconus corneas.

The observed decrease in collagen mass in the cone region of both keratoconus corneas supports both clinical and experimental findings of maximal thinning in this region [17-19]. It must be remembered, however, that although the maps of collagen mass distribution indicate a loss of collagen mass from the central 6.5mm region of both keratoconus corneas, this does not necessarily mean that there is a loss of collagen mass from the entire cornea; the possibility remains that collagen mass is not lost but simply redistributed to a location outside the button region.

The current findings in fact provide evidence of a loss of total collagen mass from the central 6.5mm region and also a redistribution of the remaining collagen mass within the button region. The latter is evident when the distribution of aligned collagen mass is examined as an index of orientation (relative to the total collagen mass). In the normal cornea, there is a large increase in the index of orientation in the superior-nasal and inferior-temporal quadrants (at a distance of 1.6 mm from the centre of the cornea) and also to a much lesser extent in the superior-temporal and inferior-nasal quadrants (Figure 3). It has been suggested that the increased index of orientation in the four quadrants of the normal cornea, may be due to the presence of additional aligned collagen that traverses the peripheral cornea and facilitates the flattening of the cornea prior to the limbus [6, 15]. However, both keratoconus corneal buttons differed from the normal cornea (and from each other) in terms of aligned collagen mass distribution. In the case of keratoconus button 1, which had a large, round, centrally located cone, the index of orientation increased in all four quadrants, whereas in keratoconus button 2, which had a smaller oval, inferior-temporally located, cone, the index of orientation in the 6.5 mm button region increased dramatically in the superior-nasal and inferior-temporal quadrants and was twice as high as normal within the main optical zone of the cornea.

The findings presented in this study have provided evidence that changes in the orientation and distribution of tissue mass in keratoconus corneas are related to the specific shape, size and location of the cone. The observed disruption to collagen orientation and mass distribution support a mechanism of tissue thinning in keratoconus corneas that involves inter-fibrillar or inter-lamellae slippage and tissue redistribution. Irrespective of the original cause of thinning in keratoconus, the structural changes identified in this study would likely further accelerate the progression of the disease as the biomechanical stability of the cornea is compromised.

Acknowledgements
The authors wish to thank Dr Mike MacDonald and the staff at the UK Synchrotron X-ray Source (Daresbury, UK) for help with data collection. This study received support from the Medical Research Council (#G0001033) and the Council for the Central Laboratory of Research Councils.

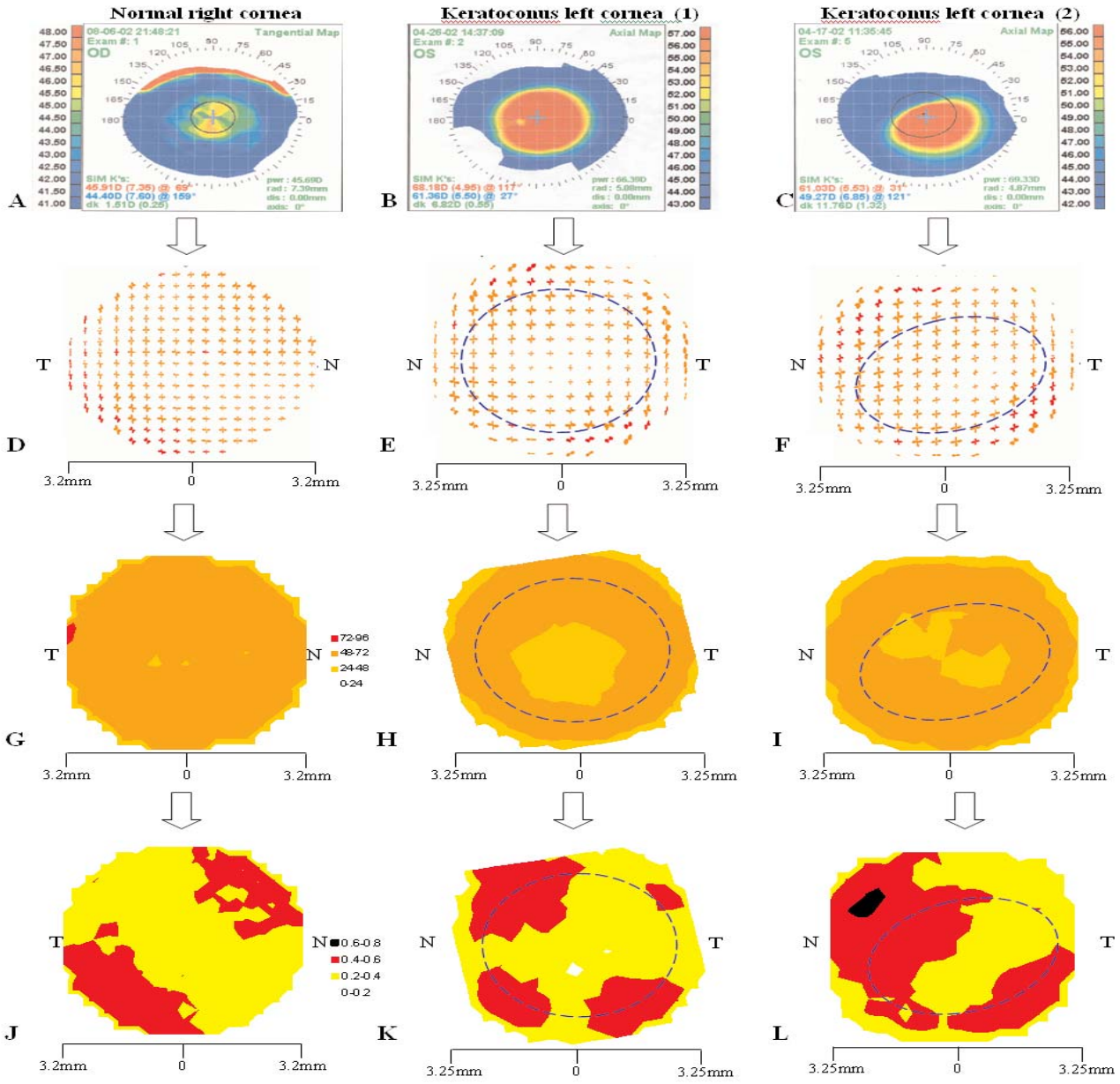

Figure 4 *Videokeratography images of a normal right cornea (A) and two left keratoconus corneas (B and C). Vector plot maps show the preferred orientation of aligned collagen in the central 6.4 mm region of the same normal right cornea (D) and the same two left 6.5 mm keratoconus corneal buttons (1 (E) and 2 (F)). Due to variations in the intensity of aligned X-ray scatter across an individual cornea (caused by variations in the amount of aligned collagen), red polar plots have been scaled down by a factor of 1.5 so that all of the vector plots can be viewed on the same map. The distribution of fibrillar collagen mass (G-I) and the index of orientation (J-L) in the same regions of the normal cornea and the two keratoconus corneal buttons are also shown. In the case of the keratoconus buttons, the region of highest dioptric power is highlighted (by a blue dashed line) in each of their respective contour and vector plot maps, to indicate the size and shape of the cone.*

References

[1] Maurice, D.M. 1957. The structure and transparenc of the cornea. Journal of Physiology 136, 263-286.

[2] Maurice, D.M. 1988. Mechanics of the cornea. In: Cavanagh, H.D. ed./eds. The cornea: Transactions of the world congress on the cornea III. New York: Raven Press Ltd. pp. 187-192.

[3] Krachmer, J.H., Feder, R.S. and Belin, M.W. 1984. Keratoconus and related non-inflammatory corneal thinning disorders. Survey of Ophthalmology 28, 293-322.

[4] Al-Yousuf, N., Mavrikakis, I., Mavrikakis, E. et al. 2004. Penetrating keratoplasty: Indications over a 10 year period. British Journal of Ophthalmology 88, 998-1001.

[5] Daxer, A. and Fratzl, P. 1997. Collagen fibril orientation in the human cornea and its implications in keratoconus. Investigative Ophthalmology and Visual Science 38, 121-129.

[6] Aghamohamadzadeh, H., Newton, R.H. and Meek, K.M. 2004. X-ray scattering used to map the preferred collagen orientation in the human cornea and limbus. Structure 12, 249-256.

[7] Boote, C., Hayes, S., Abahussin, M. and Meek, K.M. 2005. Mapping the structure of the human cornea: mirror symmetry in collagen organisation between left and right eyes. Investigative Ophthalmology and Visual Science. In Press.

[8] Meek, K.M. and Newton, R.H. 1999. Organization of collagen fibrils in the corneal stroma in relation to mechanical properties and surgical practice. Journal of Refractive Surgery 15, 695-699.

[9] Kenney, M.C. and Brown, D.J. 2003. The Cascade Hypothesis of Keratoconus. Contact Lens and Anterior Eye 26, 139-146

[10] Polack, F.M. 1976. Contributions of electron microscopy to the study of corneal pathology. Survey of Ophthalmology 20, 375-414.

[11] Ottani, V., Raspanti, M. and Ruggeri, A. 2001. Collagen structure and functional implications: A review. Micron 32, 251-260.

[12] Daxer, A. and Fratzl, P. 1997. Collagen fibril orientation in the human corneal stroma and its implications in keratoconus. Investigative Ophthalmology and Visual Science 38, 121-129.

[13] Radner, W., Zehetmayer, M., Skorpik, C. et al. 1998. Altered organization of collagen in the apex of keratoconus corneas. Ophthalmic Research 30, 327-332.

[14] Sawaguchi, S., Fukuchi, T., Abe, H. et al. 1998. Three dimensional electron microscopic study of keratoconus. Archives of Ophthalmology 116, 62-98.

[15] Meek, K.M., Tuft, S.J., Huang, Y. et al. 2005. Changes in collagen orientation and distribution in keratoconus corneas. Investigative Ophthalmology & Visual Science 46, 1948-1956.

[16] Meek, K., Blamires, T., Elliot, G. et al. 1987. The organisation of collagen fibrils in the human corneal stroma: A synchrotron x-ray diffraction study. Current Eye Research 6, 841-846.

[17] Mandell, R. and Polse, K.A. 1969. Keratoconus: Spatial variation of corneal thickness as a diagnostic test. Archived of Ophthalmology 82, 182-188.

[18] Auffarth, G.U., Wang, L. and Volcker, H.E. 2000. Keratoconus evaluation using the orbscan topography system. Journal of Cataract Refractive Surgery 26, 222-228.

[19] Liu, Z., Zhang, M., Chen, J. et al. 2002. Corneal topography and thickness in keratoconus [article in chinese]. Chung Hua Yen Ko Tsa Chih 38, 740-743.

Fibre Diffraction Review 14, 22 - 29, 2006 doi: 10.1382/fdr.2006.1405

Time Resolved X-ray Diffraction Studies of Active Bony Fish Muscle: Analysis using the New CCP13 Program FibreFix

Felicity Eakins[1], Carlo Knupp[1,2], Christian Pinali[2], Ganeshalingam Rajkumar[1], Anthony Gleeson[3], and John M. Squire[1]

1. Biological Structure and Function Section, Biomedical Sciences Division, Imperial College London, UK
2. School of Optometry and Vision Sciences, Cardiff University, Cardiff, UK.
3. CLRC Daresbury Laboratory, Warrington, Cheshire, UK

Abstract

A major task in analysing time-resolved X-ray diffraction data from contracting muscle involves processing the raw data to get it into a useful form for visualising timecourses or assessing genuine intensity or spacing changes. Here we show how the FibreFix program, including some newly incorporated or updated routines, can be used to carry out many of the necessary procedures, where possible in an automated way.

The mechanism by which muscles generate force is thought to occur through the cyclical interaction of myosin crossbridges with the protein actin. Actin and myosin form separate filaments within muscles: the thin filaments contain actin and the thick filaments contain myosin. In the contractile cycle, the crossbridges or myosin heads, which protrude at regular intervals along the thick filaments, attach to the thin filaments and undergo a conformational change associated with the hydrolysis of ATP and the release of its products. This produces a force which causes sliding of the thin filaments in between the thick filaments, if the load is not too high, and hence muscle shortening. This well known swinging crossbridge model of muscle contraction was first put forward in 1969 by Hugh Huxley (Huxley 1969) and since then a large body of work has built up in support of this theory. However, there are certain aspects of the theory which require more clarification, for example: what are the occupancies of the different states of the crossbridges during this cycle and what are the kinetics of the movement between them?

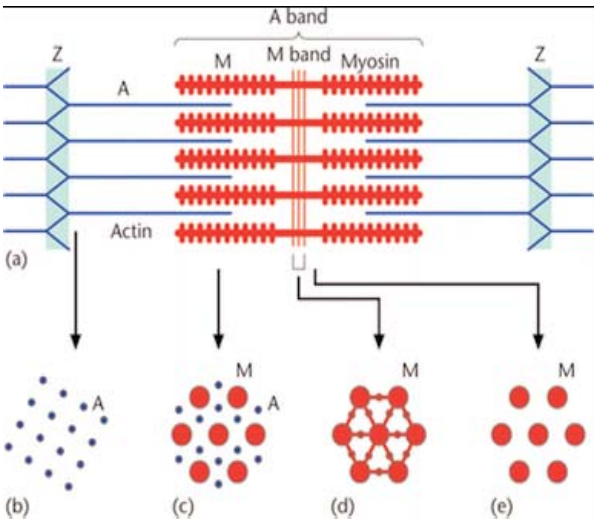

To this end, this project is applying time-resolved X-ray diffraction to intact, active, bony fish muscle. X-ray diffraction using synchrotron radiation is particularly suited to this sort of application because it can be used on live contracting muscle specimens, with high time resolution whilst still providing data with iter-order resolution. The choice of bony fish muscle for this work arises from the fact that it is very well ordered compared to other vertebrate muscles such as frog or rabbit, showing long range order and a simple 3-D crossbridge lattice (Luther, Munro et al. 1981). For this reason, bony fish muscle produces well sampled X-ray diffraction data that can be more rigorously analysed than that from other vertebrate muscles (Harford and Squire 1986). As the muscle contracts the intensities of the reflections in the X-ray diffraction pattern change as protein mass moves within the muscle sarcomere. Analysis of these changes should lead to an understanding of the moelcular movements involved in contraction.

The sarcomere is the repeating unit of striated muscle. Many sarcomeres arranged in series form a myofibril which can extend through the whole length of the muscle cell. Many myofibrils side by side form a muscle fibre. The sarcomere contains the full molecular apparatus to perform contraction. It consists of a hexagonal array of bipolar myosin filaments, anchored at the centre by the M-band, interdigitating on both halves with hexagonal ayyays of - actin filaments. These in turn are anchored to Z-lines at each end of the sarcomere (see Figure 1). Sarcomere length is measured from one Z-line to the next. During contraction the sarcomere shortens as the two sets of filaments slide in between each other.

Figure 1*: Various regions of the muscle sarcomere shown in axial view (a) and in transverse section: (b) at the Z-line (Z-band), (c) in the overlap region of the A-band, (d) at the M-band and (e) in the non-overlap region of the A-band. (A, M = actin, myosin filaments*).

Changes in the Muscle X-ray Diffraction Pattern Accompanying Contraction

i The reflections on the meridian of the pattern, labelled M3, M6 and M9 in Figure 2 are from myosin filaments. The reflections get broader and their relative intensities change.

ii The intensities of the equatorial reflections change. These give information about the muscle in a view down the filament (fibre) axis. In particular: the (1,0) reflection gets weaker and the (1,1) reflection gets stronger as the distribution of mass within the unit cell changes.

iii The myosin layer lines, which are lines of intensity parallel to the equator due to myosin (the brown reflections in Figure 2), get weaker as crossbridges move away from theor ordered arrangement on the myosin filaments to bind to actin in active muscle.

iv The actin layer lines (the blue reflections in Figure 2) get stronger due to binding of myosin heads onto the actin filaments, although not as much as in rigor muscle where all the myosin heads bind to actin.

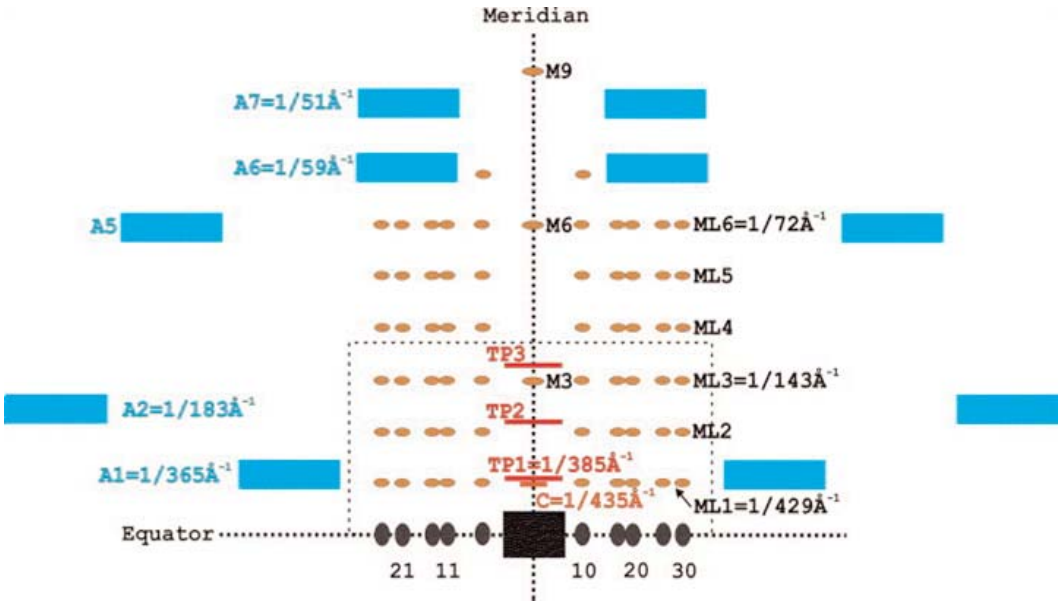

Figure 2: *Features of the low-angle X-ray diffraction pattern from relaxed bony fish muscle, taken from (Squire, Roessle et al. 2004). Blue layer-lines are from actin filaments, brown reflections from myosin filaments. Black equatorial peaks come from a view of the muscle down the fibre axis.*

This reciprocal change in strength between the two sets of layer lines occurs because in relaxed muscle the myosin layer lines come from the ordered array of myosin heads on the filament backbone, but as they move to attach to actin they loose the helical repeat of the myosin filaments and reinforce the helical repeat of the actin filament.

The intensity changes which occur during contraction, in particular those on the equator of the pattern, can be used to model the crossbridge cycle. They provide information about the changing occupancies of different states in the cycle and the kinetics of the transitions between them.

Previous work carried out on bony fish muscle has looked at these changes in conjunction with the tension timecourse produced by the muscle (Harford and Squire 1990; Harford, et al. 1991; Harford and Squire 1992). However, factors other than movements of protein domains can affect the intensities of the reflections during contraction. In particular sarcomere length changes can also affect the timecourse of tension development. Up until now the effects of any sarcomere length change which might occur during contraction of this muscle type have been neglected, because the change was thought to be small (Harford and Squire 1992). However, it is important to be able to measure and control the sarcomere length change which occurs during contraction of bony fish muscle to quantify these effects.

With this in mind, a sarcomere length control system has been developed based on monitoring muscle sarcomere length using laser diffraction. The system can measure the sarcomere length change accompanying contraction, approximately 4% reduction in length per sarcomere (47.5nm/half sarcomere), and with a feedback system can also reduce this change by about half, whilst X-ray data are being gathered. This control was observed to have an effect on the tension timecourse.

X-ray diffraction data from muscles under partial sarcomere length control and in improved physiological conditions, have been obtained on beamline 16.1 at the CLRC Daresbury Synchrotron Radiation Source. These data have been analysed using the new integrated CCP13 program FibreFix. New analysis tools have been added to the program, making the processing of time-resolved data much easier and more efficient (Rajkumar, Al-Khayat et al. 2005). Here we demonstrate some of the new functionality of FibreFix applied to the latest X-ray data from bony fish muscle under partial sarcomere length control.

Techniques

Data Collection

Time resolved X-ray diffraction data from 6 muscles (248 tetanic contractions) were obtained using the protocol in Figure 3, including some 1 ms time-frames, with the sarcomere length control system implemented on beamline 16.1 at the CLRC Daresbury Synchrotron Radiation Source with data collected on the RAPID X-ray detector.

X-ray Data Analysis

Several steps were involved in the analysis of time-resolved data using the new CCP13 program FibreFix to obtain time courses for reflections:

1. Blank cell subtraction and timecourse normalisation: BAK tool.

Muscles were mounted in thin plastic X-ray cells containing 10mls of saline solution to keep the muscle alive and functioning electrodes to stimulate the muscle to contract, and a tension transducer lever arm to measure the tension produced by the muscle during contraction. The whole X-ray cell was then placed on the X-ray beam-line. The cell has two very thin mylar windows on either side of the muscle, positioned to let the X-ray beam pass through with the least attenuation (Figure 4).

To remove any artefacts introduced into the X-ray diffraction patterns by the X-ray cell itself, diffraction patterns from the empty cell, without the muscle but containing the saline solution, were taken to be subtracted from the muscle X-ray patterns during analysis.

The count recorded by the RAPID X-ray detector for each pixel is proportional to the intensity of the X-rays incident on the pixel. However, the X-ray flux from the synchrotron is not constant, reducing with time since the last beam dump and so this needs to be compensated for. This was done with an ionisation chamber, mounted in front of the muscle, giving a total ionisation count for each frame of the timecourse, saved by the beamline acquisition system in a calibration file. The calibration file was then used to normalise the data and eliminate the effects of varying incident X-ra flux. This was done in conjuction with the removal of the blank cell using the BAK tool in FibreFix.

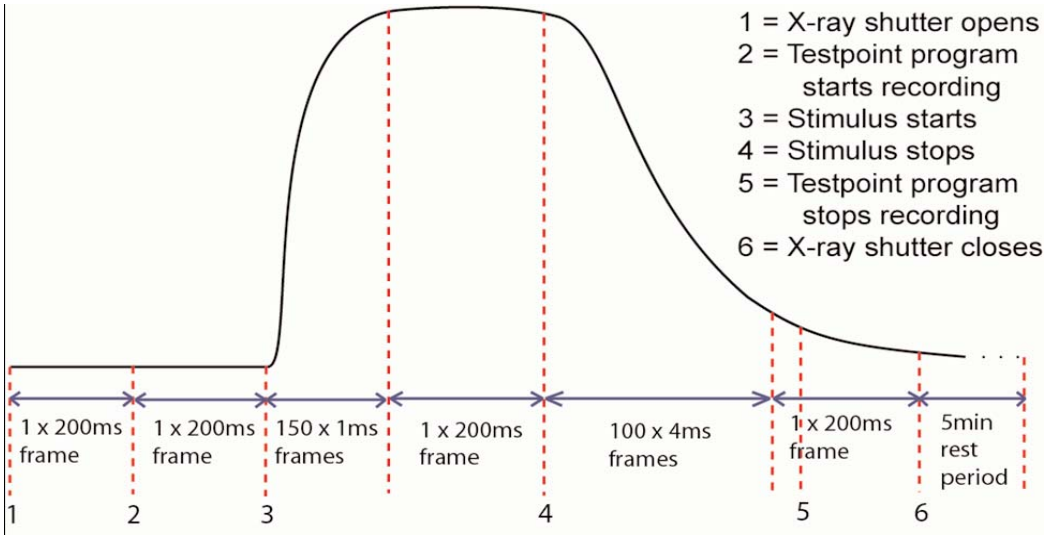

Figure 3: *Protocol for X-ray data collection from contracting bony fish muscle. Tension is plotted upwards. Time progresses from left to right. Stimulus was applied at point 3 and stopped at point 4. Number and duration of time frames when X-ray data were recorded are indicated.*

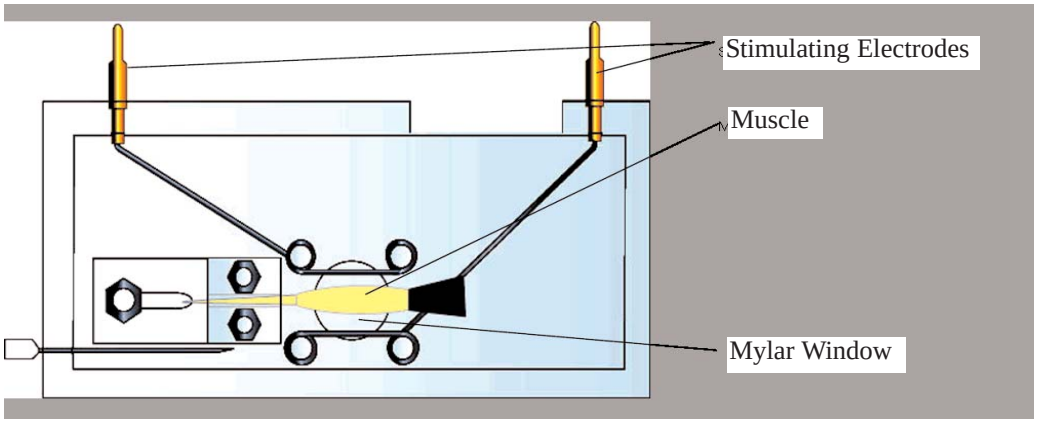

Figure 4: *Schematic illustration of the X-ray cell used for time-resolved studies of contracting bony fish muscle on beamline 16.1 at the Daresbury SRS.*

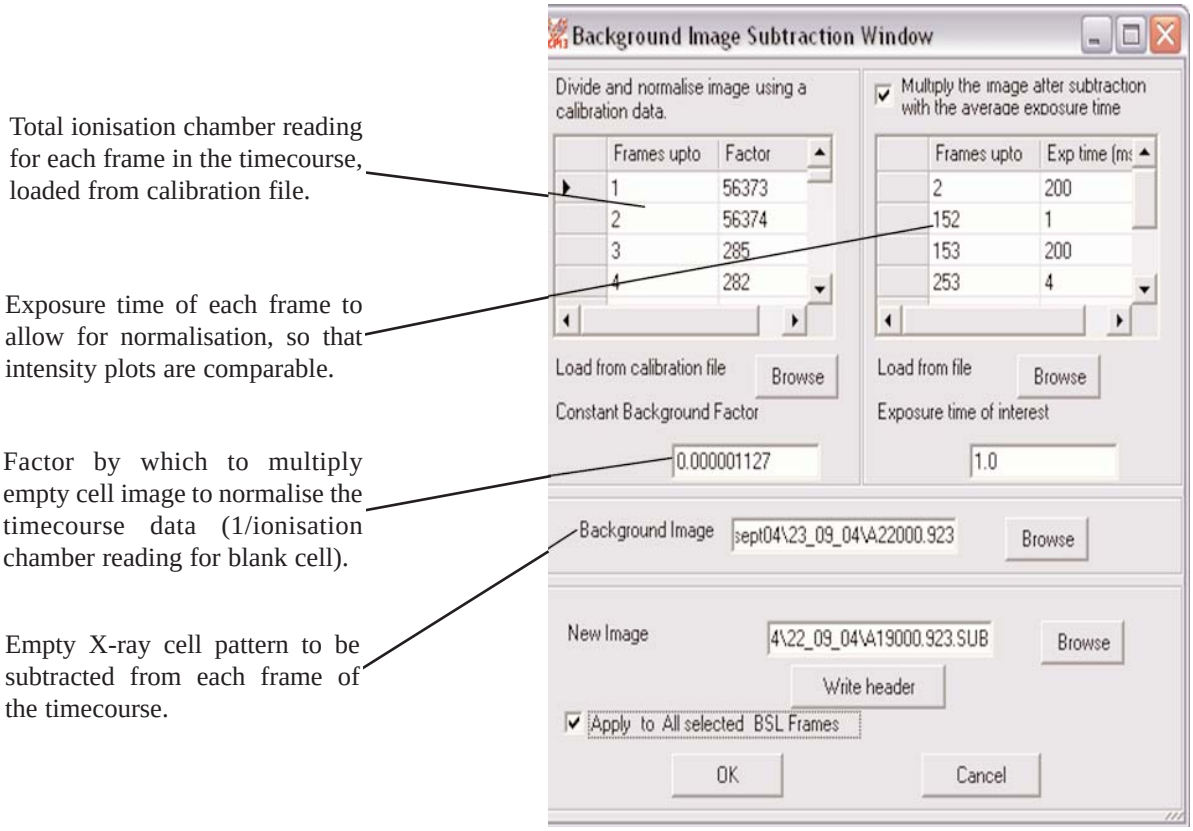

Figure 5: *The BAK tool dialogue window in FibreFix.*

The equation which this tool applies to the timecourse is:

$$\text{Normalised Timecourse Blank Cell Removed} = \left(\text{Original Timecourse Ionisation Chamber Data} - \text{CBF} \times \text{Blank Cell} \right) \times \text{Average Ionisation Count for 1 Frame}$$

Where CBF is the constant background factor.

2. Finding pattern parameters and addition of timecourses

One of the disadvantages of time resolved data is that the counts for each pixel in the shortest frames are low. To improve this, timecourses from successive contractions of particular muscles were added together and then the cumulative timecourses from different muscles were also added. However, each muscle was oriented slightly differently in the X-ray cell and so the centre and rotation of each summed timecourse needed to be aligned before addition.

Estimates of the centre and rotation for the summed timecourse from each muscle were obtained in FibreFix by selecting symmetric reflections around the centre of the pattern and then using the 'Estimate Centre' and 'Estimate Rotation' functions (Figure 6). These estimates were then refined using the 'Refine' function in the 'Process' menu to give good values for the centre and rotation of each summed timecourse. These parameters were applied to all frames in the summed timecourses using the 'Apply' button in the 'Parameter Editor' to centre and align them before summed timecourses from all the muscles were added frame by frame using the BSL SUM tool.

3. Rotation within the timecourse: PLA and PAK tools

Not only may the diffraction patterns from different muscle be rotated with respect to each other, but also the orientation of different frames in the timecourse from a particular muscle may occasionally change as the muscle contracts. This needs to be checked for and identified because all the frames of the timecourse must be aligned, centred and straightened before they can be added to a timecourse from another muscle. Two new tools in FibreFix were used to check for this effect: the PLA and PAK functions. The PAK tool allows all the patterns in a timecourse (or in any array of images) to be viewed at once by averaging pixels together to produce smaller images and then displaying all the frames in one image as in Figure 7. Any changes in rotation which occurred during the timecourse can be seen in this composite image. The PLA tool is of particular interest: it allows the user to scan through the time-series at speed, effectively watching a movie of the X-ray timecourse during contraction, again allowing any changes in rotation to be picked up. These differences in rotation between frames can then corrected using the BSL ROT tool which has been modified so that different rotations can be applied to different frames in the timecourse.

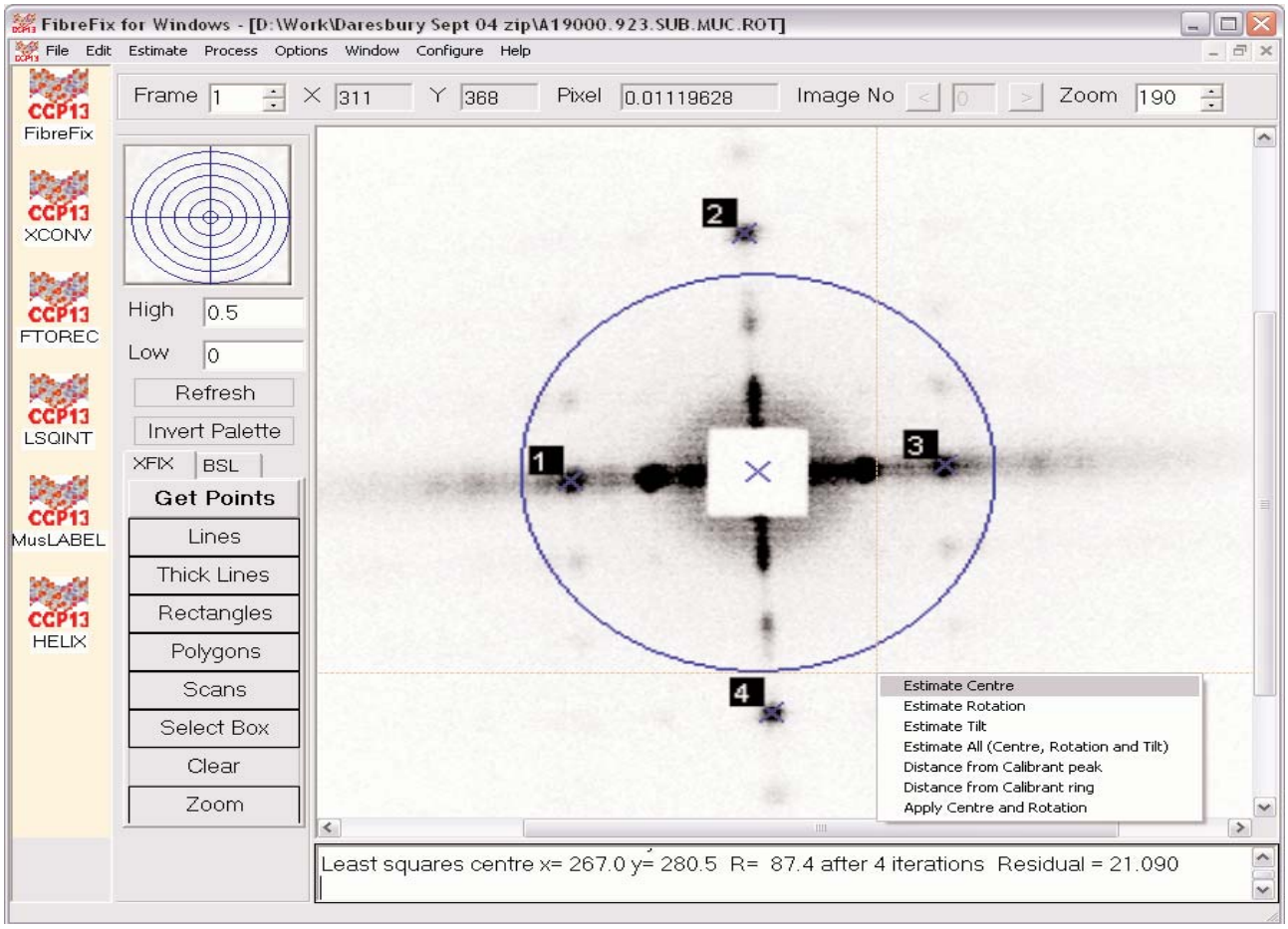

Figure 6: *Parameter Estimation in FibreFix. See text for details.*

4. Background removal

For the correct intensities of the pattern reflections to be obtained, the background scatter of X-rays has to be removed from the total summed timecourse. FibreFix uses three different methods of background fitting: Roving Window, Circularly Symmetric and Smooth. When completed, these subtract the fitted background from each frame of the timecourse. More background fitting methods are also available in the subprogram LSQINT in FibreFix, for background subtraction later in the processing.

In the present analysis the circularly symmetric and smooth background fitting tools were used. Due to the presence of some very low counts and some pixels with zero value, the short frames (in this case the 1ms time-frames frames) in the summed timecourse were difficult to fit a background to directly. It was found that the long active frame produced the best background fit i.e. with the least amount of reflection data left in it, because it has fewer reflections in the pattern due to the myosin layer lines disappearing. Therefore, the background was fitted

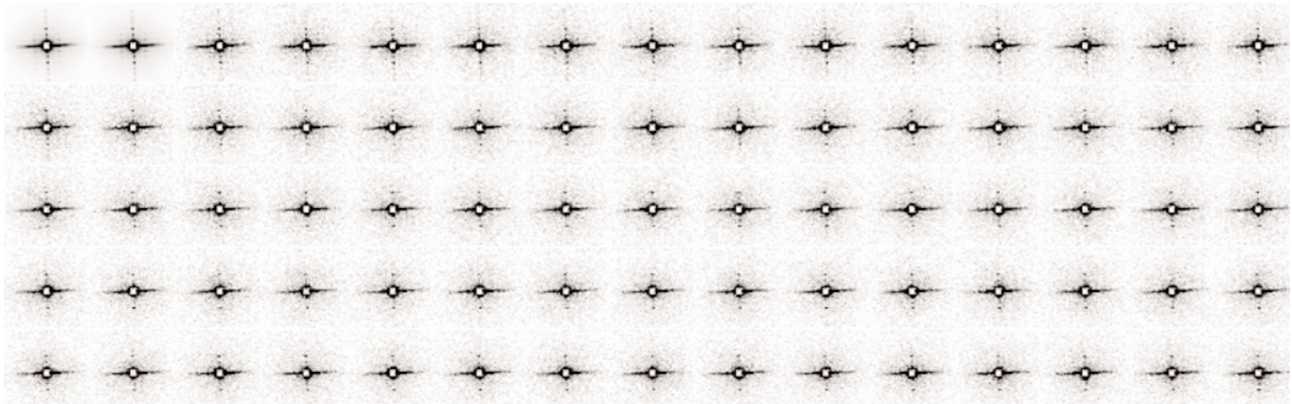

F*igure 7: Part of an image created using the PAK tool in FibreFix. Each small frame is a whole low-angle X-ray diffraction pattern from bony fish muscle (cf. Figure 8). The array can be used to assess changes in fibre orientation during a contraction.*

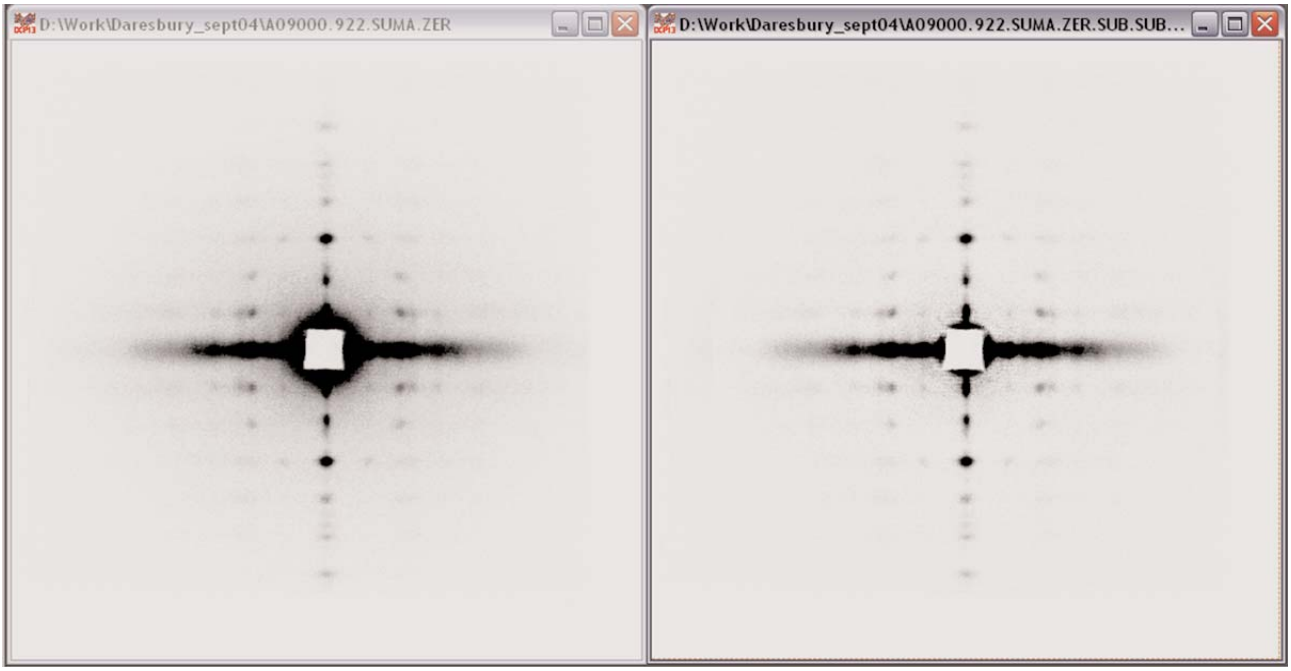

***Figure 8**: Low-angle X-ray diffraction pattern from relaxed bony fish muscle before (left) and after (right) background removal. The strong meridional spot about one-third way out from the pattern centre is the M3 peak at 1/145 Å^{-1} (cf. Figure 2).*

to the long active frame and then subtracted from all the frames in the timecourse after appropriate scaling, assuming that the background does not change greatly during the time-course.

The smooth background fitting method was applied to the timecourse first and it was then applied again to the fitted background to remove any remaining reflection data left in the background fit. This was repeated a few times to improve the fit and the final background was then subtracted from each frame in the timecourse. The circularly symmetric background tool was also used to remove the central scatter halo around the back stop.

5. Plotting reflection intensity timecourse

A new tool was developed to make this process easier in FibreFix: the TIP tool. To produce an intensity timecourse for a particular reflection in the pattern, a box was simply drawn around the reflection of interest using the TIP tool, and by clicking the right mouse button a plot was produced of the total intensity within the box with respect to the frame number. Plots for the equatorial (1,0) and (1,1) reflections were produced in this way, see figure 9.

Results

Plots of the (1,0) and (1,1) equatorial reflection intensities against frame number were produced using directly from FibreFix (Figure 9). These were obtained from the X-ray timecourse of the summed tetanic contraction of 6 muscles under 50% sarcomere length control (248 tetanic contractions).

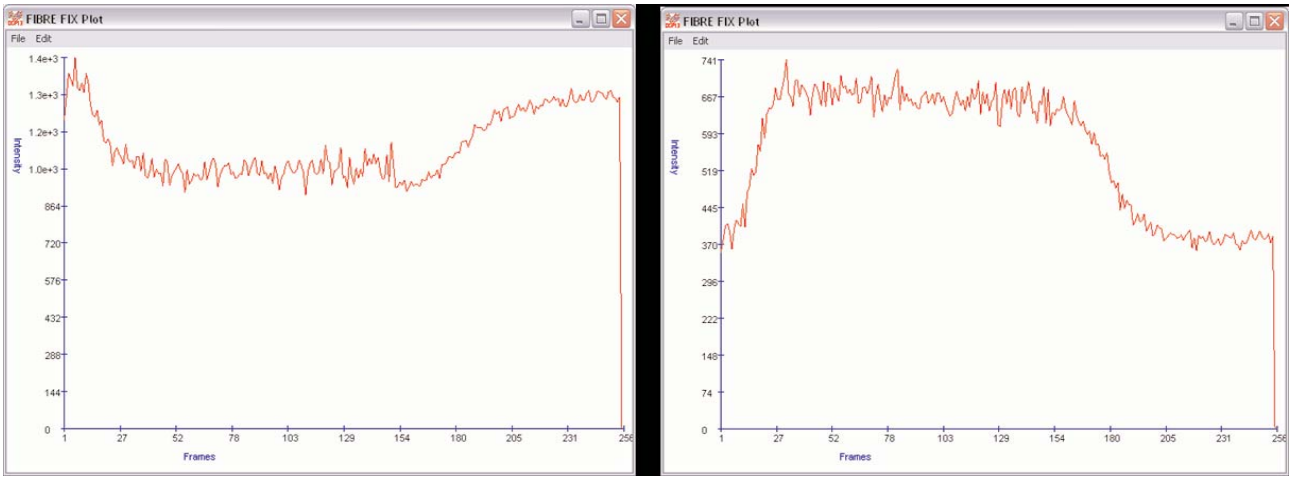

***Figure 9:** FibreFix plot of intensity changes in (1,0) (left) and (1,1) (right) equatorial reflections during the summed tetanic contraction.*

Timecourse Comparisons

The timecourses of the intensities of the (1,0) and (1,1) equatorial reflections during the first 150ms of contraction, were normalised using their average intensity during the long active frame of the timecourse. The inverse of the (1,0) reduction in intensity was taken to allow timecourses to be more easily compared. These normalised timecourses were then plotted with the normalised, average timecourse of tension development for all the summed contractions (Figure 10).

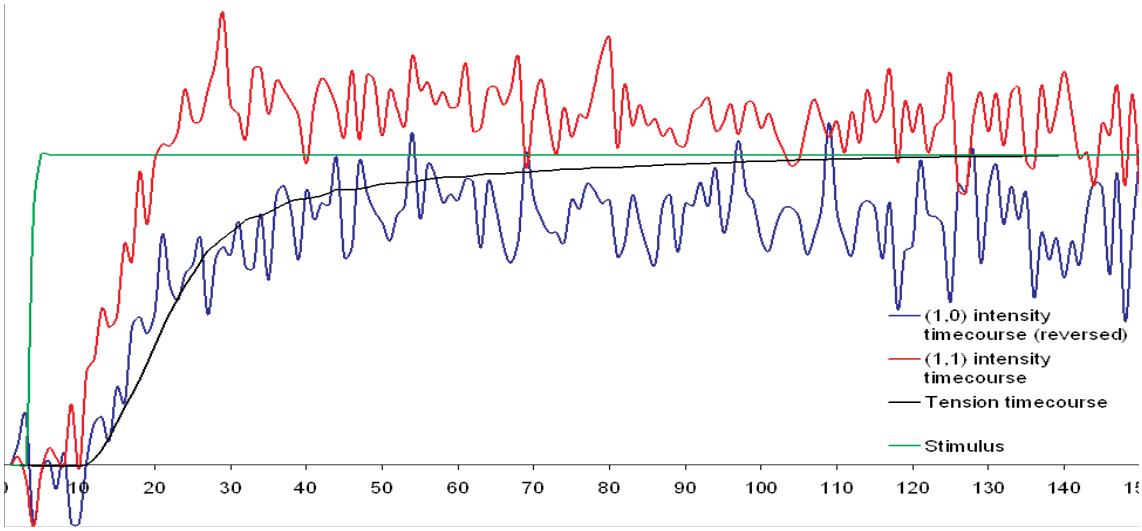

Figure 10: *Plot of the normalised intensity changes of the blue (1,0) (inverse change) and red (1,1) equatorial reflections and the tension produced (black during the rising phase of contraction in bony ifsh muscle.*

Comparing these results with previous work on vertebrate muscle, several features are of course the same (Figure 11). As tension develops:

i the (1,0) reflection gets weaker
ii the (1,1) reflection gets stronger
iii the (1,1) reflection leads tension and initily over shoots its steady state value

Conclusions and Future Work

A sarcomere length control system has been developed and implemented and has measured the sarcomere length change which accompanies tetanic contraction in bony fish muscle as a 4% reduction per sarcomere. The system with feedback included is also able to halve this sarcomere length change allowing X-ray data to be obtained under this control. The preliminary results presented here

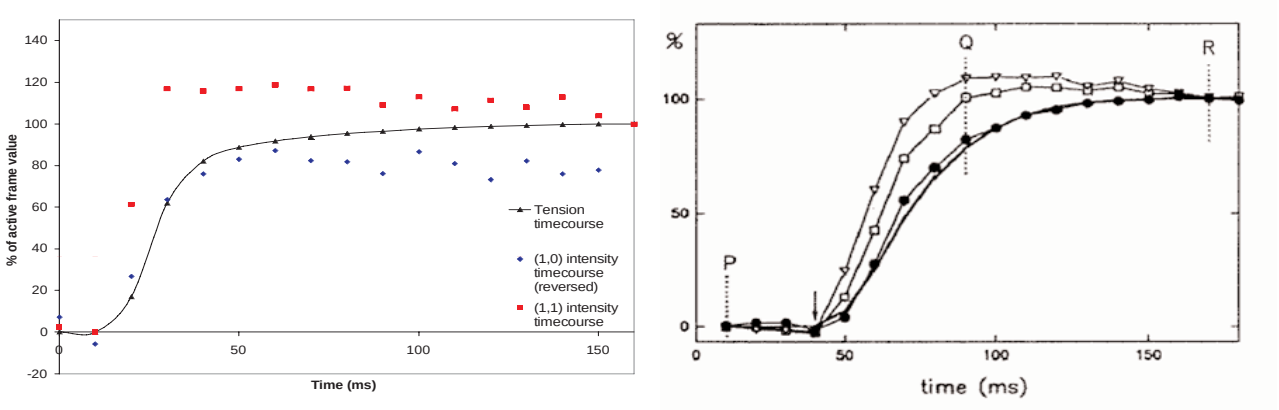

Figure 11: *comparison of normalised timecourses on a longer timebased (left) with previously published data from fish muscle (Harford and Squire 1992) (right).*

However, there are some features which are different. The (1,0) reflection initially follows the rise in tension

generally agree with the X-ray data published in previous work on bony fish. No huge changes were expected with the use of the partial sarcomere length control. Cecchi et al reported no obvious difference in the intensity time-courses from sarcomere length clamped and unclamped single frog fibres in their 1991 paper (Cecchi, Griffiths et al. 1991). More data are needed to clarify the differences seen in the timecourses from both reflections in this recent data from bony fish msucle.

New X-ray data have now been obtained from muscles both under partial sarcomere length control and without any control and these still need to be analysed as described here. The (1,0) and (1,1) timecourses which will be obtained from the new data, along with those from other equatorial reflections, can then be used to model the crossbridge cycle with both partially controlled and uncontrolled sarcomere length changes. This will help to determine any differences the reduction in sarcomere length change may be causing in the X-ray pattern and crossbridge cycle.

References

Cecchi, G., P. Griffiths, et al. (1991). "Time-resolved changes in equatorial x-ray diffraction and stiffness during rise of tetanic tension in intact length-clamped single muscle fibers." Biophys. J. 59(6): 1273-1283.

Harford, J. J., M. Chew, et al. (1991). "Crossbridge states in isometrically contracting fish muscle: evidence for swinging of myosin heads on actin." Adv Biophys 27: 45-61.

Harford, J. J. and J. M. Squire (1986). "Crystalline myosin cross-bridge array in relaxed bony fish muscle. Low-angle X-ray diffraction from plaice fin muscle and its interpretation." Biophys J 50: 145-155.

Harford, J. J. and J. M. Squire (1990). Static and time resolved X-ray diffraction studies of fish muscle. In "Molecular Mechanisms in Muscular Contraction". (J. M. Squire Eds). Macmillam Press.

Harford, J. J. and J. M. Squire (1992). "Evidence for structurally different attached states of myosin cross-bridges on actin during contraction of fish muscle." Biophys J 63(2): 387-96.

Huxley, H. E. (1969). "Mechanism of Muscular Contraction." Science 164: 1356-1366.

Luther, P. K., P. M. G. Munro, et al. (1981). "Three-dimensional structure of the vertebrate muscle A-band. III: M-region structure and myosin filament symmetry." J Mol Biol 151: 703-730.

Rajkumar, G., H. A. Al-Khayat, et al. (2005). "FibreFix - A New Integrated CCP13 Software Package." Fibre Diffraction Review 13: 11-18.

Squire, J. M., M. Roessle, et al. (2004). "New X-ray Diffraction Observations on Vertebrate Muscle: Organisation of C-protein (MyBP-C) and Troponin and Evidence for Unknown Structures in the Vertebrate A-band." Journal of Molecular Biology 343(5): 1345-1363.

Fibre Diffraction Review 14, 30 - 36, 2006 doi: 10.1382/fdr.2006.1406

14th Annual Workshop

Talk Abstracts

Solution small angle X-ray scattering of elastic fibre proteins

Clair Baldock, Veronique Siegler, J. Louise Haston, Manfred Roessle, J Gunter Grossman, Daniel V. Bax, Stuart A. Cain, Kieran T Mellody, Andrew Marson, Matthew J Rock, Cay M Kielty and Tim J Wess

Wellcome Trust Centre for Cell-Matrix Research, Faculty of Life Sciences, Michael Smith Building, University of Manchester, Manchester, M13 9PT

The extracellular matrices of virtually all connective tissues contain a variety of microfibrillar elements of which fibrillin microfibrils are a major component. These polymers are essential structural elements of matrix and act as a lattice for elastin deposition during elastic fibre formation. Fibrillin microfibrils are extensible polymers which endow connective tissues with long-range elasticity and have widespread distributions in both elastic and non-elastic tissues. They are critically important in maintaining the integrity of tissues such as blood vessels, lung and skin, both in terms of their key roles in linking cells and matrix macromolecules and in the specific biomechanical properties they impart. Linkage of the fibrillin-1 gene to the heritable connective tissue disorder Marfan syndrome, which is associated with severe cardiovascular, ocular and skeletal defects, further highlights its importance.

The molecular pathway of fibrillin microfibril assembly remains poorly understood. Intermediates have proved difficult to identify due to the large size of fibrillin molecules and their propensity to form disulphide-bonded aggregates. Knowledge of the primary structure of fibrillin has also proved difficult to translate into an understanding of supramolecular organisation or mechanical properties. Therefore, we have used small angle X-ray solution scattering to analyse the structure of nine overlapping recombinant protein fragments covering 90% of the 330kDa human fibrillin-1 molecule. We were able to calculate molecular envelopes and perform computational modelling to obtain important structural details that give information of the shape and topology of contiguous groups of domains of fibrillin-1. These data highlight the flexible nature of the proline-rich region, suggesting a role in the molecular basis of fibrillin-1 elasticity. This study has provided new insights into the conformation of tandem repeats of cbEGF domains in solution, the modular structure of fibrillin-1, and the possible arrangement of fibrillin-1 in microfibril organization.

Fibre Diffraction Analysis of Potyviruses

Gerald Stubbs, Justin Junn, Amy Kendall, Michele McDonald, Lauren Parker, David Gore

Center for Structural BiologyVanderbilt University, Nashville, TN 37232, USA
BioCAT, CSRRI Illinois Institute of Technology, Chicago, IL 60616, USA

Potyviruses are flexible filamentous plant viruses, responsible for half the viral crop damage in the world. In addition, they have great potential as vectors in biotechnology. Because of their flexibility and tendency to form disordered aggregates in solution, no fibre diffraction patterns of potyviruses have been published. This is in sharp contrast to the situation for the much more tractable potexviruses and tobamoviruses.

We have obtained disoriented but nevertheless informative diffraction patterns from partially oriented sols of wheat streak mosaic virus. We have obtained more informative diffraction patterns, with well-defined layer lines to beyond 4 %C5 resolution, from dried fibres of bean common mosaic virus (BCMV). Oriented sols were prepared by slow centrifugation in capillary tubes, followed by exposure to strong (up to 18.8 Tesla) magnetic fields. Dried fibres were also prepared in magnetic fields, at ambient humidity and under controlled humidity. Diffraction data were collected at the BioCAT beamline at APS, Argonne. These data have enabled us to determine the most probable symmetry of WSMV and BCMV, and to obtain preliminary information about the internal structure of BCMV.

Virus structure research supported by NSF grant MCB-0235653 and USDA grant 2003-01178. Fibre diffraction methods research supported by NSF Research Coordination Network grant MCB-0234001. Use of the APS supported by the U.S. Department of Energy under contract W-31-109-ENG-38. BioCAT is a NIH-supported Research Center RR-08630.

Introduction to FibreFix - The new Integrated CCP13 software package

John M. Squire

Biological Structure & Function Section, Biomedical Sciences Division, Imperial College London, London SW7 2AZ, UK

The new CCP13 program FibreFix (for Windows) has been developed to make processing of non-crystalline diffraction patterns simpler for existing users and less intimidating for new users. FibreFix (which supercedes the ICE package) incorporates the functionality of the CCP13 analysis programs XCONV, XFIX, FTOREC and LSQINT and it also includes the diffraction simulation programs HELIX and MusLABEL. This talk will introduce the FibreFix program, it will demonstrate its application to a number of different kinds of diffraction data, and it will provide a background for those wishing to try out the program themselves during the Workshop.

For further details of the CCP13 philosophy behind this program see:
Squire, J.M., AL-Khayat, H.A., Arnott, A., Crawshaw, J., Denny, R., Diakun, G., Dover, S.D., Forsyth, V.T., He, A., Knupp, C., Mant, G., Rajkumar, G., Rodman, M.J., Shotton, M. & Windle, A.H. (2003) New CCP13 software and the strategy behind further developments: Stripping and modelling of fibre diffraction data. Fibre Diffraction Review 11, 7-19.

For further details of the FibreFix program see:
Rajkumar, G., AL-Khayat, H.A., Eakins, F., He, A., Knupp, C. & Squire, J.M. (2005) FibreFix - A New Integrated CCP13 Software Package. Fibre Diffraction Review 13, 11-18.

Ultra small angle scattering at high brilliance beamlines using compound refractive lenses

M. Drakopoulos

Diamond Light Source, Chilton, Oxfordshire OX11 0DE

Refractive x-ray lenses have recently been applied for imaging and scanning microscopy with hard x-rays. We report the application of refractive lenses in an optical scheme for ultra-small angle x-ray diffraction, performed at a high brilliance synchrotron radiation source. An experimental proof of principle and a theoretical discussion are presented. In particular, we observe the x-ray diffraction pattern from a two-dimensional photonic crystal with 4.2 μm periodicity, which normally is employed to scatter light in the infra-red [1].

[1] M. Drakopoulos, A. Snigirev, I. Snigireva, J. Schilling, Appl. Phys. Lett. 86, 014102 (2005).

Collagen organisation in normal and diseased human cornea

Craig Boote, Sally Hayes, Keith M. Meek

School of Optometry and Vision Sciences, Redwood Building, King Edward VII Avenue, Cardiff, CF10 3NB

The cornea, the clear window at the front of the eye, is the principal refractive component of the human visual system. Correct focussing of light onto the retina is highly dependant on corneal shape, which in turn is governed by a layered network of mechanically reinforcing collagen fibrils. We have used wide-angle x-ray fibre diffraction to map the orientation and mass distribution of fibrils over a pair of normal human corneas. The maps indicate that corneal collagen fibrils are organised in a highly specific, anisotropic manner and that, moreover, left and right eyes display structural mirror symmetry about the central body axis. The results have implications for refractive surgery and corneal transplantation. In addition we present equivalent data from eyes with keratoconus, a condition where abnormal collagen organisation is associated with tissue thinning and a conical, astigmatic cornea.

Evolutionary Algorithms *for *Fibre Diffraction Analysis

Dr David Cairns, Dr Graeme Cameron, Prof Tim Wess, Prof Andrew Miller

University of Stirling

Evolutionary algorithms are increasingly being recognised as an important optimisation tool. They provide a very flexible method for locating optimal solutions to complex problems within a realistic time frame. This talk provides an overview of using one family of evolutionary algorithms - the genetic algorithm, to search for optimal solutions which relate to observed X-ray diffraction data from fibrillar collagen. In particular, two studies are presented demonstrating how the general principle can be applied to different problem areas. The first study examines the process of developing an optimal fit for intensities within overlapping Bragg reflections, the second

study looks at the more complex issue of determining axial rise in the molecular structure of collagen using data observed from X-ray diffraction images. The results of the two studies are presented and some general conclusions drawn concerning the suitability of using evolutionary algorithms for fibre diffraction analysis.

A wholly synthetic muscle

AJ Ryan, CJ Crook, P Topham, RAL Jones, JR Howse, A Parnell, M Geoghegan

Department of Chemistry and Department of Physics and Astronomy, University of Sheffield, UK

Applications of scattering and reflectivity will be discussed in the context of the development of generic molecular devices based on responsive polymers.

A Landolt pH-oscillator based on a bromate/sulfite/ferrocyanide, with a room temperature period of 20 min and a range of 3.1pH7.0, has been used to drive periodic oscillations in volume in a pH-responsive, polyelectrolyte hydrogel. The gel is coupled to the reaction and changes volume by a factor of at least 6. A continuously stirred tank reactor was set-up on an optical microscope and the reaction pH and gel size monitored. The cyclic force generation of this system has been measured directly in a modified JKR experiment.

The responsive nature of polyelectrolyte brushes, grown by surface initiated ATRP, have been characterised by AFM, neutron reflectivity and single molecule force measurements.

Triblock copolymers, based on hydrophobic end-blocks and either polyacid or polybase, have been used to produce polymer gels where the deformation of the molecules can be followed directly by SAXS and a correlation between molecular shape change and macroscopic deformation has been established. The power developed by these synthetic muscles has been measured.

Chemical contrast by SAXS and NMR in nano-ceramics

Rudolf Winter[(1)], Daniel Le Messurier[(1)], Chris Martin[(2)]

(1) Materials Physics, University of Wales Aberystwyth, Wales
(2) CLRC Daresbury Laboratory, Warrington, England

We report here on small angle x-ray scattering experiments performed under in-situ heating conditions at beamline 6.2 at Daresbury, combined with two-dimensional NMR results obtained at UWA. Sol-gel prepared Al2O3 and ZrO2 nanoparticles were mixed with a powdered silicate (Na2Si3O7) glass, pelletised, and heated up to 1000C while acquiring data at photon energies of 8.3keV and near the absorption edge of zirconium, 18keV. Macroscopic grain surface scattering following Porod's law is subtracted from the raw data. The evolution of the scattering pattern reveals changes of the morphology of the interface during the nucleation and initial growth of the particles from sub-nanometer size to a few nm median radius. The roughness of the scattering interfaces, interpreted by a fractal model, decreases during the annealing process. Larger product particles with smoother interfaces are formed above about 550C.

NMR results show that aluminium atoms migrate from tetrahedral site in the nucleating particles through octahedral interface sites towards tetrahedral sites when dissolved in the glass matrix.

The use of NMR (27Al) and near-edge SAXS (Zr K-edge) provides chemical contrast over a wide length range from the atomic to the particle scale, and both techniques are now available as in-situ experiments at high temperature.

Microbeam diffraction from hair and skin

Naoto Yagi, N. Ohta, H. Iwamoto and K. Inoue

SPring-8/JASRI

BL40XU at SPring-8 is called "High Flux beamline" because it uses an undulator radiation without monochromatization [1]. By focusing with two mirrors, the flux density is about 1x10^17 photons/sec/mm^2, which is suitable for a microbeam experiment using a pinhole. With a 5-micron pinhole, the flux is still about 1x10^12 photons/sec. In order to record small-angle diffraction, it is necessary to use a guard pinhole to avoid scattering from the edges of the collimating pinhole. A microbeam with a 5-10 micron diameter is routinely used. The most commonly measured specimens are hair (especially cuticle [2]) and skin (stratum corneum) in which several cosmetic companies are also interested. The microbeam is used for recording small-angel diffraction from single fibres of polymers, myofibrils, and frozen hydrated biological specimens [3]. It is also used in speckle experiments (photon correlation spectroscopy).

1. K. Inoue et al., "Present Status of high flux beamline (BL40XU) at SPring-8." Nucl. Instrum. Meth. A467-468:674-677 (2001).
2. N. Ohta et al. "Structural Analysis of Cell Membrane Complex of a Hair Fibre by Micro-beam X-ray Diffraction." J. Appl. Cryst. 38:274-279 (2005).

3. H. Iwamoto et al. "X-ray microdiffraction and conventional diffraction from frozenhydrated biological specimens." J. Synchrotron Rad. (in press).

High overall throughput detector systems for scattering experiments

Lipp J.

G-05 R63, CCLRC Rutherford Appleton Lab, Chilton, Didcot, Oxon, OX11 0QX, UK.

The trend of synchrotron radiation sources is towards producing higher flux x-ray beams. This in turn provides the opportunity for collecting good quality measurements in shorter time periods. Many real-life processes occur quickly and the study of these is well matched to high intensity beams. In order to fully exploit the opportunities offered by newer beamlines, detector systems must be capable of collecting high intensity spots/cones as well as being able to operate at high frame rates. This talk will focus on a detector suite which is being developed for incorporation in the non-crystalline diffraction beamline, I22, on the Diamond Light Source.

X-ray beam conditioning for SAXS

Karsten Joensen

JJ X-Ray Systems

The performance of a pinhole SAXS system depends critically on the choice of source, optics, pinholes, beamstops and distances. In this presentation, general guidelines for individually optimizing such performance will be presented, as well as some tricks to get the maximum flexibility out of a system once the larger design decisions have been made.

Scanning SAXS/WAXS of hierarchical fibre composites: recent experiments and future perspectives

Oskar Paris

MPI Colloids and Interfaces, Department of Biomaterials Golm Berlin

Advanced materials with directional mechanical properties are mostly fibre composites. They are frequently hierarchical structured, covering several length scales from the molecular or unit cell level to several hundreds of microns. The most prominent examples of outstanding hierarchical complexity are biological tissues such as bone, for instance, but also many man-made composites fall into this category. Recent developments of microbeam instrumentation at third generation synchrotron radiation sources allows to image the SAXS/WAXS signal from thin slices of such materials with a real-space resolution corresponding roughly to the beam size (i.e., down to the sub-micron regime). Apart of nanostructure mapping, in-situ mechanical testing combined with microbeam SAXS/WAXS allows to address local deformation mechanisms of composites at a specific hierarchical level.

The present contribution reviews some recent microbeam SAXS/WAXS studies of different hierarchical fibre composites. Results from the imaging of nanostructural parameters such as shape, size and orientation of fibres or particles in biological tissues are presented. Moreover, in-situ mechanical testing of single carbon fibres, and here in particular a unique combination of in-situ bending with X-ray nanobeam scanning is demonstrated. Finally, a short status report about instrumentation and experimental possibilities at the new SAXS/WAXS/Fluorescence beamline at BESSYII in Berlin will be given. A future challenge will be in particular the development of high-throughput on-line data reduction and visualization, limiting currently scanning microbeam SAXS/WAXS from being widely recognised as a real imaging technique.

Pressure-jump Studies of Liquid-crystalline Cubic Phase Transitions in Lipids

J. M. Seddon, C. Conn, O. Ces, X. Mulet, A. Squires, A. Heron and R. H. Templer
J. Kraineva, J. Woenkhaus and R. Winter, S. Finet and T. Narayanan

Department of Chemistry, Imperial College London, London SW7 2AY, U.K.
University of Dortmund, Physical Chemistry I, D-44227 Dortmund, Germany
ESRF, BP 220, 38043 Grenoble Cedex, France

Lyotropic liquid crystals of 1-, 2-, or 3-dimensional periodicity spontaneously assemble when biological amphiphiles are mixed with solvent under various conditions of temperature, pressure and hydration. The mesophases formed include the fluid lamellar (L/1-D), hexagonal (HI/HII/2-D) and inverse bicontinuous cubic phases (QII/3-D). Biologically, the fluid lamellar phase is ubiquitous, being the structure upon which cell membranes are based. However the inverse bicontinuous cubic phases have become increasingly accepted as not only being present in many cell membranes, but as facilitating a number of vital cell processes including endo- and exocytosis, fat digestion

and membrane budding, as these involve changes in membrane topology. These cubic phases consist of a lipid bilayer draped on mathematical surfaces known as the primitive P (space group Im3m), double-diamond D (space group Pn3m) or gyroid G (space group Ia3d) periodic minimal surfaces, subdividing 3-D space into two interpenetrating, but unconnected, water networks. The lattice parameters of these cubic phases are typically in the range 100 - 300 Å.

Previous studies of lyotropic phase transitions have concentrated on transformations between lamellar structures and between lamellar to inverse hexagonal structures, with remarkably little work being done on transitions involving cubic phases. However, a complete understanding of the physical processes governing such transitions, including the nature of any intermediates formed, and the mechanistic routes taken, is essential if we are to further our knowledge of their possible roles in fundamental cellular processes involving membranes. As a result we have recently introduced the pressure-jump technique to investigate lyotropic phase transitions by studying the rate and mechanism of the transitions in monoglyceride/water and fatty acid/phospholipid/water systems by monitoring the complete time evolution of these structural conversions. The use of pressure as a trigger mechanism has several advantages: 1) the solvent properties are not significantly altered; 2) pressure propagates rapidly meaning that equilibrium is achieved rapidly; and 3) pressure-jumps can be both in the pressurisation and depressurisation directions. A 1 kbar change in pressure typically shifts most lipid transition temperatures upwards by 20 - 30°C.

We will describe some of our recent time-resolved X-ray results obtained using beamline ID02 at the ESRF, Grenoble. Data reduction was done in part using the programs developed and implemented by Dr. P. Bösecke and colleagues at the ESRF, and in part using an IDL-based 'AXcess' X-ray analysis package developed (by A. Heron) in our laboratory in Imperial College London.

Breast Cancer Diagnosis Using Laboratory Based Small Angle X-ray Scattering, Preliminary Results.

A.R. Round, S.J. Wilkinson, C.J. Hall, K.D. Rogers, O. Glatter, T. Wess, I.O. Ellis

Department of Materials and Medical Sciences, Cranfield
University, Swindon, SN6 8LA, UK.

Previous work has indicated that breast tissue disease diagnosis could be performed using small angle x-ray scattering (SAXS) from a synchrotron radiation source. The technique would be more useful to health services if it could be made to work using a conventional x-ray source. Tumour tissue, and normal tissue from bi-lateral mastectomy procedures were examined using small angle x-ray scattering from a laboratory based source. Consistent and reliable differences in x-ray scatter distributions were observed between diseased and normal tissue samples using the laboratory based SAXSess system. Albeit from a small number of samples, a sensitivity of 100% was obtained. An encouraging result for implementing SAXS as a laboratory based diagnosis technique.

Nucleation and growth of iron oxyhydroxide nanoparticles in contaminated land environments

Sam Shaw

Department of Earth Sciences, University of Oxford, Oxford, UK

Poorly ordered iron oxyhydroxide minerals (e.g. goethite, FeOOH) are a key constituent of soils and oxidised sediments. These phases control the speciation and transport of many trace components, including pollutants (e.g. arsenic), in many natural systems, due to their abundance, high surface area and reactivity. The kinetics and mechanisms of iron oxyhydroxide precipitation and crystallisation is poorly understood primarily due to their rapid formation rates (seconds – minutes), hydrated nature and nanoparticulate size which makes characterisation using traditional high vacuum ex situ techniques (e.g. TEM) difficult. In this study, we have used in situ time-resolved Small Angle X-ray Scattering (SAXS) in conjunction with a stopped-flow cell to characterise the kinetics and mechanisms of poorly-ordered iron oxyhydroxide from solution.

The initial nucleation and growth of poorly-ordered iron oxyhydroxide was studied using SAXS in conjunction with a rapid mixing stopped-flow cell on station 6.2 of the SRS (Daresbury Laboratory). With this system we are able collect scattering patterns from dilute suspension in seconds, and therefore characterise the formation process in detail. Analysis of the SAXS data indicates that the initial precipitate consists of approximately spherical or disc shaped particles <5nm in size. The particle radii increase to 20Å during the precipitation process with growth occurring predominantly in one direction by either direct precipitation or oriented aggregation. The precipitation rate increases with increasing pH, but decreases when phosphate is present due to the adsorption of the phosphate onto the growing particles.

The development of an online data analysis toolkit for x-ray scanning micro-diffraction experiments

Manfred Burghammer

European Synchrotron Radiation Facility

The Scanning X-ray micro-diffraction method has been applied to many scientific problems mainly in the field of soft condensed matter research [1]. High spatial resolution can be obtained by scanning different positions on the specimen with a micro beam which can be as small as 0.5 microns and less. The measurment positions are usually but not necessarily arranged in a grid. The data taken at each sampling point consists of two-dimensional diffraction patterns (primary images) typically recorded with a CCD-Detector (MarCCD, 2048x2048 pixels, 16 bit per sample, ~8Mb per pattern). Parameters of interest like peak positions, interated intensities, and d-spacings have to be extracted from the primary images. These values can be assembled to secondary images representing a mapping of the selected parameter on the sample. On the Quest for high resolution mappings typically huge datasets have to be recorded. About 20 Giga-Byte (2500x8Mb) of raw data have to be processed in order to obtain a 50x50 pixel secondary image. It turned out that software becomes more and more a limiting factor. Many experiments could benefit from data processing results obtained in parallel to the data acquisition. This information should be used to give feedback to the measurement control. Exposure times could be optimized. Sample regions showing interesting features can be explored in more detail and regions with low information content could be skipped.Kinetics studies could be enhanced and it would be possible to correct for sample drifts which cannot be avoided for some dynamic experiments involving mechanical deformation for instance. Many more examples could be listed here. In order to address these problems the data processing software has to exhibit "online" capability. We are currently developing a software dedicated to the kind of "online data analysis" problems sketched above. As we are dealing with a large variety of different samples and instrumental setups the software has to be very versatile and user friendly at the same time. Therefore we chose a modular aproach implementing an online data analysis kit (ODAK). In this contribution various online data analysis aspects will be discussed and the current development status of ODAKwill be presented.

[1] New avenues in X-ray microbeam experiments Riekel C. Rep. Prog. Phys. 63, 233-262 (2000)

Present Capabilities and Future Plans for Fibre Diffraction and Small-Angle Solution Scattering at the BioCAT Facility at the Advanced Photon Source

Tom Irving

BioCAT, Dept. BCPS, Illinois Institute of Technology, 3101 S. Dearborn St. Chicago IL., 60616 USA

The BioCAT undulator beamline 18ID at the Advanced Photon Source, Argonne IL., USA, was designed from the outset to be very high performance instrument for small-angle fiber diffraction and scattering. It has been very successfully used for small-angle fiber diffraction since 1998. Over the last three years we have been developing our small angle solution scattering program which is now the fastest growing user group. Another new direction is wide-angle fiber crystallography and micro-fibre diffraction. An overview of our present capabilities will be presented with selected applications. I will also present an overview of optics and detector upgrades planned for the coming year.

Non-Crystalline Diffraction at EMBL-Hamburg - Present State and Future Plans

M. Roessle, M. Petoukhov, P. Konarev, S. Mylonas & D. Svergun

EMBL-Hamburg, Notkestrasse 85, D-22603 Hamburg

The X33 beamline at the EMBL-Outstation in Hamburg is a dedicated beamline for biological small angle scattering. It serves since more than 25 years a wide variety of users from structural biology for standard SAXS/WAXS experiments. Recent developments in computing of low resolution models from solution scattering allow a more detailed interpretation based on these SAXS/WAXS data. In order to fulfil the needs of the continuously growing user community the X33 beamline is upgraded during the period 2004 and 2005, implementing advanced components to increase the instrument sensitivity and resolution. In further steps the experimental setup will changed to allow a more automated operation. For this aim the existing data analysis software will be integrated and combined with the data acquisition system.

This upgrade of the X33 beamline goes in line with the plans for the new BIOSAXS beamline at the third generation synchrotron PETRA III project on the Hamburg

DESY site. The proposed SAXS/WAXS instrument will gain on the excellent beam parameters of the upgraded storage ring PETRA III and state-of-the-art X-ray optics such as multilayer monochromators, Kirk-Patrick-Baez optics will permit experiments in smaller volumes on shorter timescales. The BIOSAXS project comprises dedicated setups for non-crystalline diffraction of biological macromolecules and is part of the integrated life science center proposed by the EMBL Hamburg Outstation.

Fibre Diffraction Review 14, 37 - 47, 2006 doi: 10.1382/fdr.2006.1407

14th Annual Workshop

Poster Abstracts

X-ray and Neutron scattering on soft objects in a thermotropic liquid crystal

G.Toquer, G.Porte, M.Nobili, J.Appell, C.Blanc

Laboratoire des Colloïdes, Verres et Nanomatériaux UMR 5587, Université Montpellier II, CC026 Place Eugène Bataillon, 34095 Montpellier Cedex 5

In a first attempt, Tanaka [1] has studied the formation of inverted micelles of didodecyldimethylammonium bromide (DDAB) plus water in the liquid crystal 5-cyanobiphenyl (5CB) as solvent. This author has claimed the existence of a new mesophase (a "transparent nematic" phase [1]) located between the isotropic and the nematic phases, which consists of random micelles embedded in a small-scale nematic matrix. This result has been controverted by Bellini [2] who has shown by a light scattering method that there was no transparent nematic phase in this system. Nevertheless, an interesting behaviour in the isotropic micellar phase is observed. With decreasing temperature, this phase is destabilized in the neighbourhood of the isotropic/nematic transition by paranematic fluctuations which give rise to an intermicellar attractive interaction.

For a better understanding, we have characterized the lyotropic organisation by X-rays and neutron scattering far above the nematic-isotropic transition of the liquid crystal. From quantitative analyses of experimental datas we obtain the shape and size of inverted micelles.

Furthermore, there are Van der Waals interactions between micelles in this system which prevent the formation of original mesophases (lamellar phase for example). We plan to add new surfactants which could reduce the VdW interactions in order to obtain original mesophases in 5CB.

References:

[1] J.Yamamoto and H.Tanaka, Nature (London) 409, 321 (2001).

[2] T.Bellini, M. Caggioni, N.A. Clark, F.Mantegazza, A.Maritan, and A. Pelizzola, Phys. Rev. Lett. 91, 8 (2003).

Phasing of Equatorial X-ray diffraction Pattern from Drosophila Indirect Flight Muscle

John Costello and Tom Irving

BioCAT and Dept. BCPS, Illinois Institute of Technology

The equatorial portion of a fiber diffraction pattern gives information on the projection of the electron density onto a plane perpendicular to the long fiber axis. In the muscle community, changes in the intensity of the 1,1 equatorial reflection relative to the 1,0 reflection (I11/I10) in vertebrate muscle or the I2,0 /I10 in insect muscle have long been used as a qualitative measure of changes of the relative amount of crossbridge mass associated with the thin filament relative to the thick when muscles change state. If the phases of the higher order equatorial reflections can be estimated, electron density maps may be calculated allowing a more sophisticated level of analysis. The indirect flight muscle of Drosophila is a highly ordered system giving up to 14 equatorial reflections (5,1) or about 90 nm resolution. This is too low a resolution to give useful filament dimensions but may give qualitative indications about changes in dimensions. Since electron density maps are based on all the available be intensity data can yield more realistic estimates of mass shifts than I20/I10. Here we approached the phase problem using a combination of methods. The first method was to approximate the equatorial projection of the electron density as cylindrical regions of electron density with electron densities in various regions based on up to date literature values for lattice spacing along with the geometry of the unit cell. At this low resolution, centro-symmetry can be assumed and relatively crude models can be justified. By Fourier transforming these density distributions, the predicted intensities can be calculated and fit to experimental data using a Differential Evolution (DE) algorithm to minimize chi-squared. The simulation gives predicted phases for the reflections that were compared to those obtained from Fourier transformation of electron micrographs. These two phase sets were found to differ only for the (2,1), (2,2), and (5,0) reflections (which are all weak) To resolve the phase differences, electron density maps were calculated for each set of phases (EM and simulation) for data taken from skinned fibers at varying degrees of lattice spacing. The simulation phase set gave more realis-

tic changes in electron maps with lattice shrinkage than the EM phase set. Electron density maps showed a hollow center in the thick filaments using the simulation intensities and phasing. The thick filament appeared to be compressed at high degrees of lattice compression probably due to the compressibility of the hollow core. The radial extent of the myosin heads also was reduced with increasing lattice shrinkage. The simulation predicts that the crossbridges are not near the actin filaments during the relaxed state and a uniform distribution of myosin heads around the backbone. Temperature factor type disorder in the thick and thin filament was very low. Supported by the U.S. National Institutes of Health.

X-Ray Diffraction experiments to study the structural ordering of hybrid organic-inorganic sol-gel materials

J.J.E. Moreau, P. Dieudonné, L. Vellutini, J-L. Bantignies, J-L. Sauvajol, C. Bied, M. Wong Chi Mana

Laboratoire des colloïdes, verres et nanomatériaux, Bât 11, CC 026, Université MontpellierII, Place Eugène Bataillon, 34095 Montpellier Cédex 5, France and Ecole Nationale Supérieure de Chimie de Montpellier, Laboratoire Hétérochimie Moléculaire et Macromoléculaire (UMR-CNRS 5076), 8 rue de l'école normale,34296 Montpellier, France

Powder X-ray diffraction experiments have been performed to analyse the structural order of urea-based alkylene bridged silsesquioxanes with various carbon chain lengths. The results show that the organisation of the organic fragments in these hybrid silica is greatly influenced by the increasing length of the alkylene chain, the H-bonding of the urea groups and depends also on the reaction conditions.

Recent results from in/ex-situ x-ray microdiffraction studies of microdeformation induced by indentation applied to polymer fibres

A.Gourrier*, M.C. Garcia-Guttierez, C.Riekel*****

* Max-Planck Institute of Colloids and Interfaces, Biomaterials dpt., D-14424 Potsdam, Germany
**Instituto de Estructura de la Materia (CSIC),Macromolecular Physics dpt., E-28006 Madrid, Spain
***European Synchrotron Radiation Facility, B.P. 220, F-38043 Grenoble Cedex, France

The results presented in this poster demonstrate, for the first time, the feasibility of combined studies of microindentation and scanning X-ray microdiffraction (WAXS) techniques in-situ (real-time)[1]. For this purpose, a dedicated microindentation device was developed on the microfocus beamline of the ESRF (ID13). First experiments were focused on polymer fibres even though the method can also be applied to other materials such as biomaterials or metals. In-situ experiments showed that at least a part of the crystalline domains within the volume probed in the X-ray beam tend to orient in the stress field induced by the indenter during deformation (i.e. while the load is applied)[1]. Furthermore, the original crystalline orientation is almost fully recovered upon releasing the stress on the diamond tip, and should therefore be associated with elastic relaxation. Ex-situ experiments, on the other hand, showed that the orientation is partly retained in the immediate vicinity of the tip where the stress is highest, giving rise to strong textures[2,3]. Another important consequence of indentation was found in the form of phase transformations occurring in two high-performance fibres[1,2,3]. Particular emphasis is put on recent results obtained using Vectra liquid-crystalline fibres [4].

[1] A. Gourrier, M.C. Garcia, C. Riekel, Macromolecules, 35, 8072, 2002
[2] C. Riekel, M.C. Garcia, A. Gourrier, S. Roth, Anal. Bioanal. Chem., 376, 594, 2003
[3] M.C. Garcia, A. Gourrier, C. Riekel, J. Macro. Sci., B 43, 267, 2004
[4] A. Gourrier, M.C. Garcia, C. Riekel, Macromolecules, 38, 3838, 2005

The polymer network of wood cell walls: an examination by small-angle X-ray scattering and X-ray diffraction

Karin Jungnikl, Oskar Paris, Ingo Burgert, Peter Fratzl

Department of Biomaterials, Am Mühlenberg 1, D-14476, Potsdam-Golm, Germany

The three structurally relevant groups of polymers in wood cell walls are cellulose, lignin and hemicelluloses. Our aim is to gain more insight into the function of hemicellulose and lignin, the matrix polymers in which the cellulose fibrils are embedded. Slices of spruce wood (Picea abies [L.] Karst.) were subjected to chemical treatments, which degrade and remove lignin and hemicelluloses to varying degrees and, as a consequence, have a specific effect on the swelling behaviour and aggregation of the cellulose in the cell wall. The used chemical agents were sodium chlorite (NaClO2) for delignification, sodium hydroxide at different concentrations for removal of hemicelluloses and an acidic hydrogen peroxide solution, which removes most of the cell wall matrix. The corresponding structural changes of the cell wall were observed by small-angle scattering (SAXS) and wide-angle diffraction (WAXS), in the wet (never dried) state and after drying. While mere delignification had only little effect on the swelling and drying behaviour of the cellulose fibrils, the structural changes upon increasing degradation of the hemicelluloses were severe.

SAFs: self-assembled protein fibres of de novo design

David Papapostolou, Maya Pandya, Max Ryadnov, Andrew Smith & Derek Woolfson

Department of Biochemistry, School of Life Sciences, University of Sussex, UK

Self-assembling systems are found extensively in biology, An improved understanding of these would fuel efforts to engineer novel, bioinspired materials through de novo design. Coiled-coil motifs provide simple systems for studying molecular self-assembly. We have designed two 28-residue peptides to assemble into extended coiled-coil fibres. Complementary peptide-peptide interactions were used to direct the folding of a "sticky ended" heterodimer as a building block for the assembly of long fibres. Assembly was monitored in solution using circular dichroism spectroscopy. Furthermore, fibre formation was confirmed by electron microscopy, which revealed linear non-branched structures, tens of μm long and ~50 nm thick. This thickness is ~20 greater than expected for the two-stranded coiled-coil target. One explanation is that the two-stranded structures are nascent protofibrils that bundle to form the matured, thick fibers. X-ray fibre diffraction of partially aligned samples gave patterns indicative of coiled-coil structure, and also suggested that the protofibrils packed to form a highly ordered, hexagonal lattice. The use of fluorescently labelled peptides showed that the fibres were polar, as the labelled molecules incorporated specifically to one end of the fibres. Redesign of the peptides resulted in an increase in order, thickness and thermal stability of the fibres. Furthermore, the design of non-linear peptides based on the original peptide has provided insight into how fibre morphology can be controlled. These findings show that the self-assembled fibres are rich in structure and information, and that they present possibilities for the bottom-up assembly of new nanostructured functional biomaterials.

Time Resolved X-ray Diffraction Studies of Active Bony Fish Muscle: Analysis using the New CCP13 Program FibreFix

Felicity Eakins[1], Carlo Knupp[1&2], Christian Pinali[2] and John M. Squire[1]

1. Biological Structure and Function Section, Biomedical Sciences Division, Imperial College London, UK
2. School of Optometry and Vision Sciences, Cardiff University, Cardiff, UK

The well known swinging crossbridge model of muscle contraction was first put forward in 1969 by Hugh Huxley and since then a large body of work has built up in support of this theory. However, there are certain aspects of the theory which require more clarification, for example: what are the occupancies and kinetics of the different states of the crossbridges during this cycle To this end, this project is employing time-resolved X-ray diffraction to intact, active bony fish muscle. X-ray diffraction has the advantage over other methods of studying muscles in that it can be used on live contracting muscle specimens whilst still providing data with high spatial resolution [Squire et al., 2003]. Bony fish muscle is being used in conjunction with X-ray diffraction because it is very well ordered compared to other vertebrate muscles such as frog, showing long range order and a simple 3-D cross-bridge lattice.

Previous work carried out on bony fish muscle has looked at the changes which occur in the X-ray pattern during contraction in conjunction with the tension timecourse produced by the muscle. Up until now the effects of any sarcomere length change which might occur during the contraction of this muscle have been neglected because the change was thought to be small [Harford & Squire, 1992]. However, sarcomere length changes can have an effect on both the timecourse of tension development and the timecourse of intensity changes of the X-ray reflections from the muscle. Therefore, it is important to be able to measure and control the sarcomere length change which occurs during contraction of bony fish muscle to quantify these effects.

With this in mind, a sarcomere length control system has been developed based on monitoring muscle sarcomere length using laser diffraction. The system can measure the sarcomere length change accompanying contraction and can also reduce this change by about half, whilst X-ray data are being gathered. This control has had an effect on the tension timecourse. X-ray diffraction data from muscles under partial sarcomere length control and in improved physiological conditions have been obtained and are now being analysed using the new integrated CCP13 program FibreFix. New analysis tools have been added to this program, making the processing of time resolved data much easier and more efficient [Rajkumar et al., 2005]. This poster demonstrates some of the new functionality of FibreFix applied to the latest X-ray data from bony fish muscle under partial sarcomere length control.

Harford, J.J. & Squire, J.M. (1992) "Evidence for structurally different attached states of myosin crossbridges on actin during contraction of fish muscle" Biophys. J. 63: 387-396

Squire, J.M., Knupp, C., AL-Khayat, H.A. & Harford, J.J. (2003) "Millisecond time-resolved low-angle X-ray diffraction: a powerful, high-sensitivity technique for modelling real-time movements in biological macromolecular assemblies." Fibre Diffraction Review 11: 28-35.

Rajkumar, G., AL-Khayat, H., Eakins, F., He, A., Knupp, C. & Squire, J.M. (2005) "FibreFix - A New Integrated CCP13 Software Package" Fibre Diffraction Review (in press).

Nanoscale assemblies of aligned polyfluorene films

Matti Knaapila[1], Mika Torkkeli[2], Benjamin P. Lyons[1], Ritva Serimaa[2], Oliver H. Seeck[3], and Andrew P. Monkman[1]

1. Department of Physics, University of Durham, South Road, Durham DH1 3LE, UK.
2. Department of Physical Sciences, POB 64, FI-00014 University of Helsinki, Finland.
3. HASYLAB am DESY, Notkestrasse 85, D-22605 Hamburg, Germany.

We report on the design of anisotropic structures of liquid crystalline pi-conjugated polymer, PF2/6 polyfluorene, including a subtle issue of crystal orientation. At a threshold molecular weight Mn*10 kg/mol, PF2/6 has a phase transition between hexagonal and nematic phases[1] separating low (Mn Mn*) and high (MnMn*) molecular weight regimes which affects both alignment[2] and surface morphology[3]. In aligned films on rubbed polyimide, the rigid PF2/6, taking the helical axes parallel to crystallographic c axis, lies on the substrate pointing in the rubbing direction (denoted z here). The aligned film shows two differently oriented coexisting crystallite types in-plane. Type I have crystal axis a normal to the surface (x) and type II along the substrate surface (y)[4-5]. This organization leads to a large absorption and dispersion of the refractive index in the (xy0)-plane with respect to the x axis[6].

[1] Knaapila et al. Phys. Rev. E. (2005) 71 041802
[2] Knaapila et al. Macromolecules (2005) 38 2744
[3] Knaapila et al. Adv. Funct. Mater. (2005) in press
[4] Knaapila et al. J. Phys. Chem. B (2003) 107 12425
[5] Knaapila et al. J. Phys. Chem. B (2004) 108 10711
[6] Lyons & Monkman J. Appl. Phys. (2004) 96 4735

Sulphotransferase mutations and corneal matrix structure

Andrew J. Quantock[1], Yasutaka Hayashida[2], Nicola Beecher[1], Robert D. Young[1], Philip Lewis[1], Keith M. Meek[1], Bridgeen Kerr[3], Bruce Caterson[3], Akira Tanigami[4], Tomoya O. Akama[5], Michiko N. Fukada[5], Yasuo Tano[2], Kohji Nishida[2]

1. Structural Biophysics Group, Cardiff School of Optometry and Vision Sciences, Cardiff University, Cardiff, UK.
2. Department of Ophthalmology, Osaka University Medical School, Osaka, Japan.
3. Connective Tissue Biology Laboratory, Cardiff School of Biosciences, Cardiff University, Cardiff, UK.
4. Otsuka GEN Research Institute, Otsuka Pharmaceutical Co. Ltd., Tokushima, Japan.
5. Glycobiology Program, The Burnham Institute, La Jolla, California, USA.

Keratan sulphate (KS) glycosaminoglycans (GAGs) substituted on proteoglycans (PGs) are key constituents of the extracellular matrix of the corneal stroma where they are believed to help govern collagen fibrillar ultrastructure. Corneas of mice lacking the KSPGs lumican and keratocan show structural matrix changes, whereas the corneal stroma in mice with a null mutation for the other corneal KSPG, mimecan, is minimally affected. To assess the role of KS GAG sulphation in the control of collagen matrix structure in cornea we generated mice with null mutations in Chst5, a gene encoding an N-acetylglucosamine-6-O-sulphotransferase (GlcNAc6ST) that is integral to the sulphation of KS chains. This gene is an ortholog of CHST6, which in humans encodes for a GlcNAc6ST and is causative for macular corneal dystrophy (MCD), a recessive condition characterised by progressive corneal clouding. Chst5+/- ES cells were generated by homologous recombination using a target vector that contained a genomic DNA fragment of Chst5 with a neo expression cassette which replaced a protein encoding exon of the gene. Chst5 null mice were generated by intercrossing Chst5+/- mice originated from the targeted ES cells. Corneas of Chst5 null mice were optically clear, and even in old age showed no evidence of a murine form of MCD. The collagen fibrillar architecture of corneas from 21 mature (5-10 month) mice was studied by synchrotron x-ray fibre diffraction, and this disclosed that average collagen fibril diameters in heterozygous (35.7nm ± 0.6nm; n11), homozygous (34.9nm ± 0.7nm; n18), and wild type (36.4nm ± 0.9nm; n12) corneas were not significantly different. Average centre-to-centre fibril spacing in corneas of homozygous mutants (42.5nm ± 3.4nm; n18), on the other hand, was lower than that in wild type corneas (47.8nm ± 3.5nm; n12) and heterozygous corneas (48.3nm ± 2.2nm; n11), and these differences were highly significant (p0.001). Local order in the fibrillar array, as indicated by the coherence distance, was lower in corneas of homozygous mutants (184nm ± 19nm; n18) than heterozygous mutants (236nm ± 13nm; n11) or wild types (247nm ± 18nm; n12). Thus, despite the fact that KS in mouse cornea has less highly sulphated epitopes than KS in the corneas of other, larger mammals the discovery of structural matrix changes in homozygous Chst5 null mice points to a role for KS sulphation in the control of collagen fibril arrangement in mouse cornea.

An X-ray Diffraction Study of Collagen Orientation and Mass Distribution in Normal and Keratoconus Corneas

S.Hayes, Y.Huang, S.Tuft, C.Boote, K.Meek

Optometry & Vision Sciences, Cardiff University, Cardiff, United Kingdom; Department of Ophthalmology, Great Wall Hospital, Bejiing, China
and
Moorfields Eye Hospital, London, United Kingdom.

Purpose:
To increase our understanding of the relationship between corneal structure and shape, we examined the structural abnormalities associated with the disease keratoconus. Keratoconus is characterised by a thinning and steepening of the cornea.

Methods:
Three keratoconus corneal buttons of 8mm diameter and three normal human corneas were tagged with a nylon suture at the 12 o'clock position, before being preserved in 10% formalin. A videokeratographic image of surface dioptric power was recorded for each cornea (in vivo for keratoconus corneas and in vitro for the normal controls). Wide angle x-ray scattering (WAXS) patterns were obtained at 0.4mm intervals over the entire area of each sample using a computer operated translation stage on Station 14.1 at the Daresbury Synchrotron Radiation Source, UK. Each WAXS pattern was analysed to produce quantitative information regarding the total amount of collagen (aligned and isotropic) and the preferred orientation of aligned collagen at a known position in the cornea. By arranging the data onto a grid of corneal position, various maps were produced to illustrate the distribution and preferential orientation of collagen in each sample. The relationship between collagen arrangement and surface topography was examined in detail for both the normal and keratoconus corneas.

Results:
The preferred orientation of collagen and the distribution of collagen mass was altered in the keratoconus corneas, and in each case the nature of the abnormalities appeared to be related to the surface topography. In the apical region of the diseased corneas, the normal orthoganol preferred orientation of collagen fibrils was absent. Also, in contrast to the normal gradual symmetrical increase of collagen from the central cornea to the periphery, maximal thinning occured in the apical region of the keratoconus corneas and an asymmetrical distribution of collagen was seen throughout the remainder of each button.

Conclusion:
The results indicate a redistribution of collagen mass in keratoconus corneas. This study therefore supports the theory that corneal thinning in keratoconus occurs as result of lamella sliding away from the apical region. The existence of this mechanism would also help to explain the altered orientation of collagen fibrils in this region.

Collagen Interfibrillar Spacing in the Developing Chick Cornea and the Influence of Keratan Sulphate

Melody Liles, Briedgeen Kerr*, Clare Hughes*, Bruce Caterson*, Andrew Quantock

School of Optometry and Vision Sciences and
*School of Biosciences, Cardiff University, Cardiff
Institute of Tissue Engineering and Repair.

PURPOSE. In the week leading up to hatch, the embryonic chick cornea thins and becomes transparent (Coulombre and Coulombre, 1958; Hay and Revel, 1969; Connon et al., 2002, 2003). Proteoglycans have long been envisaged as potential modulators of corneal structure in the latter stages of development; previous chemical quantification of glycosaminoglycans from corneal isolate has indicated no change in the amount, molecular size, or degree of sulphation between developmental days 10 and 14 (Hart, 1976). After this time keratan sulphate (KS) becomes more highly sulphated, with lumican likely bearing most of these chains (Cornuet et al., 1994; Dunlevy et al., 2000). This study aims to correlate changes in the levels of sulphated KS with collagen interfibrillar spacing in the developing chick cornea.

METHODS. Low-angle synchrotron x-ray diffraction of 78 isolated corneas from chicken embryos obtained daily from developmental day 12 to day 18 (n10 to 12 at each timepoint) was used to non-invasively measure average centre-to-centre collagen fibril spacing. Next, quantification by ELISA of papain digests of the same corneas was performed using the monoclonal antibodies 5D4 and 1B4 that recognise highly and lesser sulphated epitopes on the KS chain respectively.

RESULTS. Antigenic highly sulphated KS in the developing chick cornea (given as ug/mg wet weight of tissue (+/-SD)) measured 2.7+/-1.5 (day 12), 3.1+/-0.7 (day 13), 2.0+/-0.8 (day 14), 2.6+/-1.5 (day 15), 11.6+/-4.4 (day 16), 16.1+/-8.4 (day 17), and 24.1+/-7.9 (day 18) as quantified by 5D4. Lesser sulphated KS measured using 1B4 undergoes little change in the earlier stages of development; between days 12 and 15 levels rise from 0.29+/-0.35 to 0.52+/-0.34. After this point, levels increase more rapidly; doubling from 0.73+/-0.42 (day 16) to 1.50+/-1.04 (day 18).

Over the period studied the average collagen fibril spacing in these same corneas dropped from 65nm to 53nm, and mainly this occurred after day 15. For the data set of 78 individual corneas, collagen interfibrillar spacing and antigenic 5D4 KS levels showed a significant inverse correlation (p0.001; R20.501), accompanied by a non-significant rise in lesser sulphated KS as measured by 1B4 (p0.005, R20.3897).

CONCLUSIONS. As the secondary chick cornea develops and becomes transparent the compaction of stromal collagen fibrils is accompanied by an increase in tissue levels of sulphated KS. The remodelling of fibrillar arrangement may be related to a switch to highly sulphated KS production, however KS is unlikely to be the sole driver of this transition, which we feel suggests a possible role in "fine tuning" the fibrillar array.

Small Angle X-ray Scattering Studies of Collagen Degradation

KKW Siu[1], AR Round[2], CJ Hall[3], SJ Wilkinson[2], DE Crombie[4], M Rowley[4], KD Rogers[2] and RA Lewis[5]

1. School of Physics and Materials Engineering, Monash University, Victoria 3800, Australia
2. Department of Materials and Medical Sciences, Cranfield University, Wiltshire SN6 8LA, UK
3. Daresbury Laboratory, Warrington, Cheshire WA4 4AD, UK,
4. Department of Biochemistry and Molecular Biology, Monash University, Victoria 3800, Australia.
5. Monash Centre for Synchrotron Science, Monash University, Victoria 3800, Australia.

Recent studies have investigated the sensitivity of Small Angle X-ray Scattering (SAXS) data to detect changes in the extracellular matrix (ECM) structure in breast cancer.

Systematic differences in the axial d-spacings and intensities of X-ray scattering from the fibrillar collagens in malignant, benign and normal tissues of the human breast have been observed. These differences are hypothesised to arise from the remodelling of the ECM that is necessary for tumour growth, invasion and metastasis. These events are associated with abnormal expression of the collagenases responsible for ECM degradation. We observed the in vitro enzymatic degradation of rat tail collagen, porcine subcutaneous tissue and human breast tissue using SAXS in an attempt to further understand the ultrastructural changes that take place during breast cancer progression. The results suggest that the intensity changes previously observed in malignant tissues are the result of degradation processes but that the axial spacing changes arise from abnormal collagen formation.

2D Model Fitting to SAXS Patterns from Soft Tissue

S.J.Wilkinson, K.D.Rogers, C.J.Hall

Daresbury Laboratory, Cranfield University

Here, methods are presented to achieve 2D chi square fitting to specific features which in this case are ordered collagen peaks along with a representation of the background scatter. Requirements for much of the analysis required from soft tissues small angle x-ray scattering (SAXS) patterns, producing parameters is used to describe and simplify the data. Radially averaged 1D data is obtained. Curve fitting is then employed on resulting 1D data to extract relevant information as part of the analysis procedure. Here a simple model was used and reliably fitted to a variety of 2D diffraction patterns for which the log was first taken to reduce the data range and improve fitting accuracy. The model used to fit to log data consisted of an exponential background along with a specified number of Gaussians. When used with the 2D case the model becomes rotated about a specified centre. To achieve a reliable fit for the model, estimates from a 1D averaged sector were fitted.

The 1D curve fit estimates were supplied to the 2D fitting and with the aid of sensible data weighting and basic wavelet filtering, successful and reliable fitting of a specified 2D model is shown to be achievable. In this way multiple patterns could be fitted without the need for time consuming data minimizing and laborious curve fitting. As described the model is very simple and allows area data to be parameterized to a minimal form to extract ordered collagen information such as position. The simple model can easily be extended to achieve a more comprehensive and complex pattern fitting achieving orientation distribution functions.

An X-ray Diffraction Study on Mouse Cardiac Cross-Bridge Function in vivo : Effects of Adrenergic Beta-stimulation

N. Yagi, R. Toh, M. Shinohara, T. Takaya, T. Yamashita, S. Masuda, S. Kawashima, M. Yokoyama

SPring-8/JASRI, Department of Internal Medicine, Kobe University Graduate School of Medicine

X-ray diffraction from cardiac muscle in the left ventricular free wall of a mouse heart was recorded in vivo. After the R-wave in electrocardiogram, the ratio of the intensities of the equatorial (1,0) and (1,1) reflections decreased for about 50 msec from a diastolic value of 2.1 to a minimum of 0.8, and then recovered. The spacing of the (1,0) lattice increased for about 90 msec from the diastolic value of 37.2 nm to the maximum of 39.1 nm, and then decreased. Stimulation of beta-adrenergic receptor by dobutamine accelerated both the decrease in the intensity ratio, which reached a smaller minimum ratio, and the increase in the lattice spacing, but the intensity ratio and spacing at the end-diastole were unchanged. The recovery of the lattice spacing during relaxation was also accelerated. These results support the current view that beta-stimulation accelerates both activation and relaxation in cardiac muscle. This is the first in vivo investigation at a molecular level on how β-stimulation affects the contractility of cardiac muscle. This x-ray diffraction technique will be an excellent method to examine left ventricular contractility in live transgenic mice.

Small Angle X-ray Scattering of a lobster aorta

Veronique Siegler and Tim J. Wess

Cardiff University, School of Optometry and Vision Sciences, Biophysics Group

The aorta of primitive vertebrates and invertebrates have been shown to contain fibrillin-like microfibrils, implying that these biopolymers have had an elastic role for at least 550 million years. In mammalian tissues, fibrillin molecules assemble to form microfibrils. It remains unclear whether the important mechanical and elastic roles of fibrillin in tissues across the animal phyla occur at a molec-

ular or a suprafibrillar level. Small-Angle X-ray diffraction techniques were used to determine and compare the structure-function relationships in tissues with a phylogenetic distance. A segment of the abdominal artery of a lobster was mounted on a mechanical rig to allow tissue extension and the biomechanical testing was combined with Small-Angle-X-Ray-Scattering (SAXS) at ID02 at the European Synchrotron Radiation Facility. The fundamental axial periodicity in the unstretched lobster aorta was found to be 45nm against 56nm in the mammalian tissues. The axial periodicity increased by up to 150% in the lobster aorta against 87% in the mammalian zonular filaments, indicating a much higher elastic extension limit. The presence of meridional series and an equatorial scatter corresponding to a lateral interference function of 37nm in the unstretched lobster aorta indicated the presence of an axial periodic structure. Wess et al. (1998 and 1997) have also reported the existence of a periodic structure in the mammalian zonules. The lobster tissue extension led to a gradual shift of the lateral spacing towards higher reciprocal distance values, indicating an increased lateral packing density. When the lobster aorta tissue was tensioned by up to 70%, the axial coherence decreased, as the fibrillin-like microfibrils most probably reorganised. At a tissue stretching of 100%, the predominance of the third order in the meridional series showed an ordered microfibrillar arrangement, possibly with a one-third stagger. At tissue stretching of 130%, however, this microfibrillar arrangement was much less obvious. In the mammalian zonules, the observed third meridional peak has been found to disappear as the tissue is stretched (Haston et al., 2003). Therefore there are both commonalities and differences in the biomechanical responses of mammalian and invertebrate microfibrils-containing tissues.

Development of FibreFix A new Integrated CCP13 software package

Ganeshalingam Rajkumar, Hind AL-Khayat, Felicity Eakins and John Squire

Biological Structure and Function Section, Biomedical Sciences Division, Imperial College London, London SW7 2AZ, UK

A new Integrated CCP13 program FibreFix has been developed which incorporates the functionality of the CCP13 analysis programs XCONV, XFIX, FTOREC and LSQINT and also many important functionalities of the well-known BSL program.

FibreFix is now a complete, user-friendly, program for X-ray fibre diffraction data stripping. It incorporates a new version of LSQINT, which has been completely redeveloped with a graphical user interface (GUI), and also provides direct access to the helical diffraction simulation programs HELIX and MusLABEL

For further details of the FibreFix program see:

Rajkumar, G., AL-Khayat, H.A., Eakins, F., He, A., Knupp, C. & Squire, J.M. (2005) FibreFix - A New Integrated CCP13 Software Package. Fibre Diffraction Review 13, 11-18.

Also see tutorials on the CCP13 website: www.ccp13.ac.uk

An X-ray Diffraction Study of Collagen Orientation and Mass Distribution in Normal and Keratoconus Corneas.

S.Dennis[1], C.Boote[1], Y.Huang[2], S.Tuft[3] and K.Meek[1]

1. Optometry & Vision Sciences, Cardiff University, Cardiff, United Kingdom.
2. Department of Ophthalmology, Great Wall Hospital, Bejiing, China.
3. Moorfields Eye Hospital, London, United Kingdom.

Purpose:
To increase our understanding of the relationship between corneal structure and stability we examined the structural abnormalities associated with the disease keratoconus. Keratoconus is characterised by a thinning and steepening of the cornea.

Methods:
Three keratoconus corneal buttons of 8mm diameter and three normal human corneas were tagged with a nylon suture at the 12 o%27clock position, before being preserved in 10% formalin. A videokeratographic image of surface dioptric power was recorded for each cornea (in vivo for keratoconus corneas and in vitro for the normal controls). Wide angle x-ray scattering (WAXS) patterns were obtained at 0.4mm intervals over the entire area of each sample using a computer operated translation stage on Station 14.1 at the Daresbury Synchrotron Radiation Source, UK. Each WAXS pattern was analysed to produce quantitative information regarding the total amount of collagen (aligned and isotropic) and the preferred orientation of aligned collagen at a known position in the cornea. By arranging the data onto a grid of corneal position, various maps were produced to illustrate the distribution and preferential orientation of collagen. The relationship between collagen arrangement and surface topography was examined in detail for both the normal and keratoconus corneas.

Results:
The preferred orientation of collagen and the distribution of collagen mass was altered in keratoconus corneas; the abnormalities appeared to be related to the specific shape of each cornea. In the apical region of the keratoconus corneas, the normal orthoganol preferred orientation of collagen fibrils was absent. Also, in contrast to the normal gradual symmetrical increase of collagen from the central cornea to the periphery, maximal thinning occurred in the apical region of the keratoconus corneas and an asymetrical distribution of collagen was seen throughout the remainder of each button.

Conclusion:
The results indicate a redistribution of collagen mass in keratoconus corneas. This study therefore supports the theory that corneal thinning in keratoconus occurs as result of lamella sliding away from the apical region. The existence of this mechanism would also help to explain the altered orientation of collagen fibrils in this region.

Application of the new Integrated CCP13 Software Package FibreFix on an amyloid X-ray diffraction pattern

Hind A. AL-Khayat, Ganeshalingam Rajkumar and John M. Squire

Biological Structure and Function Section, Biomedical Sciences Division, Imperial College London, London SW7 2AZ, UK

The new, single, user-friendly CCP13 software package known as FibreFix (Rajkumar et al., 2005, Fibre Diffraction Review 13, 11-18) has been applied for the first time to an X-ray fibre diffraction pattern from amyloid fibrils formed from fragment A(11-25). This construct gives a distinctive X-ray diffraction pattern and has been analysed previously (Sikorski et al. 2003, Structure 11, 915-926) using different software for stripping the X-ray diffraction patterns. The pattern is sampled, but highly disoriented. Here we describe in detail the steps involved in using FibreFix in analysing such an amyloid X-ray pattern. This involved, centering the pattern, determining its rotation, defining the specimen tilt, fitting the background, subtracting the background, obtaining peak intensities values and defining the unit cell parameters. The intensity values can in future be used in further modelling analysis to study the arrangement of the peptide within the amyloid fibre specimen for comparison with the previously published model of Sikorski et al. (2003, as above).

Original amyloid X-ray data from Dr. Louise Serpell with permission.

Mouse Corneal Development

Jack Sheppard, Keith Meek, Marcela Votruba

Cardiff University

Murine corneal development in terms of collagen development and collagen orientation has not yet been studied. Transparency is dependent on collagen orientation. Developing murine corneas were studied at time points post natal days 7-11 to see how collagen orientation and collagen mass develop. This worl is in conjuction with looking at how the development of the cornea occurs during normal development and will later be compared to the developing corneas of keratoconic mice.

Electrospinning triblock Copolymer Ultrafine Fibers

Linge Wang, Anthony J. Ryan

Department of Chemistry,
University of Sheffield

Electrospinning is a straightforward method to produce ultra-thin fibers (tens of manometers to several microns) from polymer solutions. It could take advantage of the high surface to volume ratio to make very efficient sensors and nanotechnology devices.

In this study, he linear triblock copolymers (Kraton G1650) was solved in tetrahydrofuran (THF), and the ultrafine fiber are produce by the electrospinning the polymer solution. The morphologies and the structure properties of the polymer solutions and the electrospun fibers were investigate and compared by small-angle X-ray scattering (SAXS).

Metallocene made Isotactic Polypropylene: Flow Induced Crystallisation and Structural Transformation during Stretching

Geoffrey R Mitchell, Claudio De Rosa, Finizia Auriemma, Simona Esposito

University of Naples "Federico II" Dipartimento di Chimica Complesso Monte S. Angelo, Via Cintia 80126 Naples, Italy.
and
University of Reading, Whiteknights, Reading RG6 6AF UK.

Metallocene catalysts enable isotactic polypropylene (i-PP) to be prepared with well-defined levels of defects in terms of stereoregularity. We have used in-situ synchrotron-based small angle X-ray scattering (SAXS) experiments to probe the behaviour of these novel polymers under shear flow and during the subsequent crystallisation and during deformation in the solid state.

The SAXS data shows the development of oriented structures perpendicular to the flow direction (kebabs) and we explore the effect of different amounts of defects of stereoregularity on the crystallisation of i-PP under the influence of a shear flow field is explored. Wide angle X-ray scattering (WAXS) patterns of samples crystallised after cessation of the shear flow indicate a significant level of preferred orientation of the crystals. Moreoever, the WAXS data reveal that these structures contain disordered modifications intermediate between the a and g forms.

It has been recently shown that metallocene made i-PP samples containing high concentration of defects exhibit high levels of elasticity. The elastic recovery is associated with a reversible polymorphic transition between the mesomorphic and the a form. In-situ synchrotron-based WAXS diffraction data obtained during stretching and relaxation cycles of an i-PP sample with a high concentration of defects have shown that the g form present in the unstretched film transforms into the mesomorphic form at high deformation. The mesomorphic form transforms into the a form by releasing the tension. This transition is accompanied by an elastic recovery. For samples containing a lower level of stereoregular defects, which do not show elastic properties, no polymorphic transition is observed after releasing the tension and no elastic recovery is observed.

The use of a low molar mass self assembled template to direct the crystallisation of Poly(e-caprolactone)

Supatra Wangsoub, Geoffrey R Mitchell, Robert H Olley

University of Reading

We show that small quantities of dibenzylidene sorbitol dispersed in poly(e-caprolactone) coupled with shear flow provide a self-assembling nanoscale framework to yield high levels of crystal orientation. Under shear flow, the additive forms highly extended nano-particles which lie parallel to the flow field and on cooling, polymer crystallisation is directed by these particles. We use in-situ time-resolving SAXS and WAXS techniques to explore how this behaviour can be modified by the composition, the shear rate and strain. In-situ SAXS measurements show that during the flow an anisotropic structure develops with highly extended objects of length ~700%C5 in the flow direction and ~40-60 %C5 in the transverse direction. On cooling the SAXS patterns obtained at room temperature show the presence of a highly anisotropic lamellar structure with a long spacing of ~180%C5. The corresponding WAXS patterns show significant anisotropy in the 110 and 200 crystalline peaks. Although 1% of DBS is sufficient to produce these templating effects, increasing the level of DBS leads to increased anisotropy in the PCL crystals until the effects plateau at ~ 3%. Increasing the shear rate for the flow imposed in the melt state leads to high levels of anisotropy of both the DBS fibrils in the melt and the templated PCL at room temperature. In addition, there is an increase in the level of anisotropy with increasing shear strain with some evidence for a plateau at the highest shear strain.

In conclusion, the combination of DBS and shear flow leads to an overall morphology with a high level of PCL crystal orientation. Without the additive the PCL exhibits an isotropic microstructure. This templating represent a novel and powerful approach to effective microstructure control.

Layer Specific Collagen Orientation in Human Arteries During Tensile Testing

F. Schmid[1], G. Sommer[3], M. Rappolt[1], P. Regitnig[4], C.A. Schulze-Bauer[2*], M. Auer[2], G.A. Holzapfel[3], P. Laggner[1], H. Amenitsch[1]
*** deceased 2002**

1. Institute of Biophysics and X-Ray Structure Research, Austrian Academy of Sciences, Graz, Austria
2. Institute of Structural Analysis, Computational Biomechanics, Graz, Austria
3. Department of Solid Mechanics, Royal Institute of Technology, Stockholm, Sweden
4. Institute of Pathology, Karl-Franzens-University, Graz, Austria

The collagen diffraction patterns of human aortas under uniaxial tensile test conditions have been investigated by synchrotron small angle X-ray diffraction. Using a recently designed tensile testing device the orientation and d-spacing of the collagen fibers in the major arterial layers have been measured in situ under physiological conditions together with the macroscopic force and sample stretching. The results show a direct relation between the orientation/extension of the collagen fibers on the nanoscopic level and the macroscopic stress and strain. This is attributed first to a straightening, second to a reorientation of the collagen fibers, and last to an up-take of the increasing loads by the collagen fibers.

[1] F. Schmid et al., In Situ Tensile Testing of Human Aortas by Time-Resolved Small Angle X-ray Scattering, J.Synchr.Rad., 2005, in press.
[2] F. Schmid et al., In Situ Tensile Testing of Human Arteries, in: Elettra Science Update, April 2005, http://www.elettra.trieste.it/science/update/docs/SAXS_050323_Arteries.pdf

Fibre Diffraction Review: Instructions to Authors

Submitted original papers, technical reports, Reviews, comments/letters and meeting reports for inclusion in *Fibre Diffraction Review* are welcome.

Technical Reports

These include presentations of the latest developments in CCP13 and other fibre diffraction/ non-crystalline diffraction software and their scientific justification and also, for example, reports on developments at synchrotron beamlines used for fibre diffraction and non-crystalline diffraction studies.

Reviews

These include summary presentations of the 'state of the art' in the structural analysis of particular fibrous or non-crystalline systems.

Original Papers

These present previously unpublished results from fibre diffraction or small-angle scattering experiments using either X-ray, neutron or electron diffraction.

Expanded Poster-Prize Abstracts

At each of the CCP13/ NCD Annual Workshops cash prizes are presented to the best poster presentations. The judges are always senior scientists in the field and are often from overseas. Winners of the Poster Prizes are invited to expand their abstracts into short papers for inclusion in *Fibre Diffraction Review*.

Refereeing

All papers, of whatever category above, will be refereed by at least two people (from the CCP13 Committee or their nominated referees) and may be either (a) accepted as they stand, (b) returned for rapid revision, or (c) rejected. As well as their scientific content, papers will be judged on their clarity of presentation and the quality of their figures.

Meeting Reports

Fibre Diffraction Review includes reports on relevant meetings and conferences which include an element of fibre diffraction or small-angle scattering and which will be of general interest to our readers. Such reports will often be solicited by the Editor from known meeting participants. Other potential contributors to this part of the Journal should contact the Editor prior to writing their report.

Comments/Letters

Feedback from readers about CCP13, about the NCD community and about the Journal itself are welcome. These could be in the form of comments or letters to the Editor. Suitable contributions will be published in the Journal.

Advertisements

Industrial/commercial adverts of interest to our readers are welcome. Potential advertisers should contact the Editor for details of current rates.

Submission

Contributions should be sent to the Editor before the annual deadline (December 31st) for each issue. Contributions submitted after this date may be held over for the following issue.

Colour illustrations are welcome and are included without charge. Contributions should be submitted in electronic format to the Editor (j.squire@imperial.ac.uk).

Text should be in Word 6 format and illustrations should be submitted as separate files at high resolution in TIFF or JPG format.

References should be in the format specified for *J. Molecular Biology*, and should be complete with title. Please find more details from our website.

Reprints

It is not economic for us to produce reprints of articles. However, all papers are available on the CCP13 website in downloadable pdf format.

Editor's Address

Professor John M. Squire,
Head, Biological Structure and Function Section,
Imperial College of Science, Technology & Medicine,
London SW7 2AZ, UK.

Editor '*Fibre Diffraction Review*' (ISSN 1463-8401).

Useful World Wide Web addresses (URL)

Fibre Diffraction Review	**http://www.fibrediffractionreview.org**
CCP13	**http://www.ccp13.ac.uk**
	http://www.ccp13.org
	http://www.bio.aps.anl.gov/biocat/mirror/www.ccp13.ac.uk/
	http://www.ill.fr/ccp13
NCD	**http://www.srs.dl.ac.uk/NCD**
SRS	**http://www.srs.ac.uk/SRS**
FiberNet	**http://fibernet.us/**